Cell

Diet Diurnally Regulates Small Intestinal Microbiome-Epithelial-Immune Homeostasis and Enteritis

Graphical Abstract

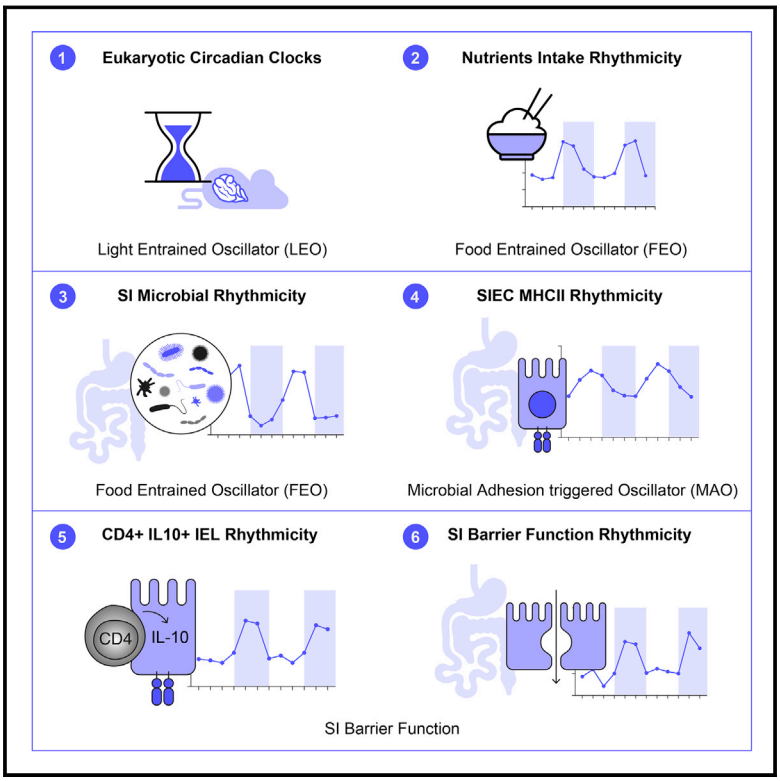

Highlights

- Small intestinal epithelial cell (SIEC) transcriptome features diurnal oscillations
- Diurnal SIEC MHC class II expression is driven by dietary timing and content and the microbiome
- SIEC MHC class II modulates diurnal SI IL-10 secretion and barrier function
- Disruption of the diurnal diet-microbiome-host axis exacerbates Crohn-like enteritis

Authors

Timur Tuganbaev, Uria Mor, Stavros Bashiardes, ..., Kenya Honda, Hagit Shapiro, Eran Elinav

Correspondence

hagit.shapiro@weizmann.ac.il (H.S.), eran.elinav@weizmann.ac.il (E.E.)

In Brief

The diurnal regulation of gut immunity depends upon the expression of MHCII induced by a population of commensal bacteria adherent to the small intestine in a diet-dependent manner.

Tuganbaev et al., 2020, Cell *182*, 1–19
September 17, 2020
https://doi.org/10.1016/j.cell.2020.08.027

CellPress

Please cite this article in press as: Tuganbaev et al., Diet Diurnally Regulates Small Intestinal Microbiome-Epithelial-Immune Homeostasis and Enteritis, Cell (2020), https://doi.org/10.1016/j.cell.2020.08.027

Cell

CellPress

Article

Diet Diurnally Regulates Small Intestinal Microbiome-Epithelial-Immune Homeostasis and Enteritis

Timur Tuganbaev,[1,14] Uria Mor,[1,14] Stavros Bashiardes,[1,16] Timur Liwinski,[1,2] Samuel Philip Nobs,[1] Avner Leshem,[1,13] Mally Dori-Bachash,[1] Christoph A. Thaiss,[1,15] Elisha Y. Pinker,[1] Karina Ratiner,[1] Lorenz Adlung,[1] Sara Federici,[1] Christian Kleimeyer,[1] Claudia Moresi,[1] Takahiro Yamada,[3] Yotam Cohen,[1] Xiao Zhang,[4,5] Hassan Massalha,[6] Efi Massasa,[6] Yael Kuperman,[7] Pandelakis A. Koni,[8,9] Alon Harmelin,[7] Nan Gao,[4,5] Shalev Itzkovitz,[6] Kenya Honda,[10,11] Hagit Shapiro,[1,*] and Eran Elinav[1,12,17,*]

[1]Immunology Department, Weizmann Institute of Science, Rehovot 7610001, Israel
[2]1st Department of Medicine, University Medical Center Hamburg-Eppendorf, 20246 Hamburg, Germany
[3]Division of Biochemistry, Faculty of Pharmacy, Keio University, Tokyo 105-8512, Japan
[4]Department of Biological Sciences, Rutgers University, Newark, NJ 07102, USA
[5]Rutgers Cancer Institute of New Jersey, New Brunswick, NJ 08901, USA
[6]Molecular Cell Biology Department, Weizmann Institute of Science, Rehovot 7610001, Israel
[7]Department of Veterinary Resources, Weizmann Institute of Science, Rehovot 7610001, Israel
[8]Georgia Cancer Center, Augusta University, Augusta, GA 30912, USA
[9]Parker Institute for Cancer Immunotherapy, San Francisco, CA 94129, USA
[10]RIKEN Center for Integrative Medical Sciences (IMS), Tsurumi, Yokohama, Kanagawa 230-0045, Japan
[11]Department of Microbiology and Immunology, Keio University School of Medicine, Shinjuku, Tokyo 160-8582, Japan
[12]Division of Cancer-Microbiome Research, DKFZ, Heidelberg 69120, Germany
[13]Department of Surgery, Tel Aviv Sourasky Medical Center, Tel Aviv, Israel
[14]These authors contributed equally
[15]Present address: Microbiology Department, Institute for Immunology, and Institute for Diabetes, Obesity & Metabolism, Perelman School of Medicine, University of Pennsylvania, Philadelphia, PA, USA
[16]Present address: Department of Molecular Virology, The Cyprus Institute of Neurology and Genetics, Nicosia, Cyprus.
[17]Lead Contact
*Correspondence: hagit.shapiro@weizmann.ac.il (H.S.), eran.elinav@weizmann.ac.il (E.E.)
https://doi.org/10.1016/j.cell.2020.08.027

SUMMARY

Throughout a 24-h period, the small intestine (SI) is exposed to diurnally varying food- and microbiome-derived antigenic burdens but maintains a strict immune homeostasis, which when perturbed in genetically susceptible individuals, may lead to Crohn disease. Herein, we demonstrate that dietary content and rhythmicity regulate the diurnally shifting SI epithelial cell (SIEC) transcriptional landscape through modulation of the SI microbiome. We exemplify this concept with SIEC major histocompatibility complex (MHC) class II, which is diurnally modulated by distinct mucosal-adherent SI commensals, while supporting downstream diurnal activity of intra-epithelial IL-10^{+} lymphocytes regulating the SI barrier function. Disruption of this diurnally regulated diet-microbiome-MHC class II-IL-10-epithelial barrier axis by circadian clock disarrangement, alterations in feeding time or content, or epithelial-specific MHC class II depletion leads to an extensive microbial product influx, driving Crohn-like enteritis. Collectively, we highlight nutritional features that modulate SI microbiome, immunity, and barrier function and identify dietary, epithelial, and immune checkpoints along this axis to be potentially exploitable in future Crohn disease interventions.

INTRODUCTION

Diet shapes intestinal physiology, through a variety of microbiome-dependent and -independent mechanisms. However, most nutritional influences have been primarily studied in the large intestine and in the context of metabolic health (Canfora et al., 2015; Cani et al., 2009; Ridaura et al., 2013; Thaiss et al., 2014, 2016, 2018; Thomas et al., 2009; Turnbaugh et al., 2006; Vrieze et al., 2012). In contrast, mechanistic understanding of dietary modulation of small intestine (SI) physiology, where the majority of dietary exposures and interactions take place remains elusive. The SI epithelial layer, comprising distinct SI epithelial cells (SIECs) and resident intra-epithelial T cell lymphocytes (IELs), is constantly challenged with extreme shifts in dietary

Please cite this article in press as: Tuganbaev et al., Diet Diurnally Regulates Small Intestinal Microbiome-Epithelial-Immune Homeostasis and Enteritis, Cell (2020), https://doi.org/10.1016/j.cell.2020.08.027

influences throughout the course of a day. During waking hours, peaking nutrient availability mandates rapid adaptation of SIEC absorptive functions, balanced with immune tolerance toward increased antigenic burdens associated with food intake. Opposite conditions are present during the resting phase. The crosstalk between SIECs and IELs includes SIEC uptake of luminal antigens (Büning et al., 2005; Gonnella and Wilmore, 1993; Ladinsky et al., 2019), their processing (Hershberg et al., 1997), presentation to T cells (Vezys et al., 2000; Westendorf et al., 2009), and, reciprocally, regulation of $Lgr5^{+}$ SIEC stem cell differentiation by T cell-derived cytokines (Biton et al., 2018). However, how SIECs and IELs cooperate in coping with the daily fluctuations in food intake and related antigenic exposures, maintaining the crucial equilibrium between the host's nutritional and immune demands, remains largely unknown.

A breakdown of this poorly understood SIEC circadian adaptation to changing environmental cues may lead to immune dysregulation, culminating in immunopathology among individuals with underlying genetic susceptibilities to auto-inflammatory disorders. For example, Celiac disease is characterized by an uncontrolled auto-inflammation in genetically predisposed individuals, which is driven by a gluten-containing diet (Lázár-Molnar and Snyder, 2018) and ameliorated by gluten-free diet (Cummins et al., 1991). Likewise, exclusive enteral nutrition (EEN) has long served as an empiric management therapy of pediatric Crohn disease (CD) (Ashton et al., 2019). However, the mechanism by which dietary interventions help in shaping the SI immunity in homeostasis and in CD remains unknown.

Likewise, most gut microbiome research has been predominantly focused on the large intestinal microbial community and its proxy, the fecal microbiome, while modulatory dietary activities related to the distinct SI microbiome (Suez et al., 2018; Zmora et al., 2018) remain understudied. In the large intestine, circadian rhythm constitutes a major organizational principle of homeostatic diet-host-microbiome cooperation (Chaix et al., 2014; Gil-Lozano et al., 2016; Thaiss et al., 2014, 2016; Tognini et al., 2017; Zarrinpar et al., 2014), while breach of large intestinal microbiome circadian homeostasis leads to a concomitant microbial and host dysfunction, contributing to metabolic disease (Thaiss et al., 2014; Zarrinpar et al., 2014). Whether similar circadian organizational principles apply to SI host-microbiome cooperative adaptation to diurnally shifting environmental conditions, including diet, remains unknown. In this study, we sought to explore these interactions and their potential impacts on SI immune homeostasis and risk of development of CD.

RESULTS

Determining Dietary Influences on SIEC Transcriptional Landscape

Throughout this section, results pertaining to pooled experiments derive from independent repeats performed under identical conditions, available at https://data.mendeley.com/datasets/wp2wt38pdg/draft?a=1bb5fe57-453f-4b05-b558-3207bb705b8a. We began our investigation by characterizing the transcriptomic landscape (by RNA sequencing) of sorted jejunal small intestinal epithelial cells (SIECs, $CD45^{-}$ $EpCAM^{HI}$) of male 12-week-old C57BL6 mice, kept in specific pathogen-free (SPF) versus germ-free (GF) conditions, or collected at the peak (ZT12) versus trough (ZT0) time points of SI absorptive activity (Pan and Hussain, 2009; Figure 1A). SIECs were further compared to colonic intestinal epithelial cells (Figure 1A). Transcriptome comparison between SIECs collected from SPF mice at the peak (ZT12) versus trough (ZT0) of SI absorptive activity revealed 114 changing Gene Ontology (GO) terms ($q < 0.1$), suggesting a diurnal nature of SIEC gene expression (Figure S1A). Comparison between SIECs collected at SPF versus GF conditions at ZT0 identified 254 GO terms ($q < 0.1$) to be differentially regulated by the microbiome (Figure S1B). Comparison between jejunal and colonic IECs at ZT0 revealed 57 differentially expressed SI-specific GO terms ($q < 0.1$, Figure S1C). The trilateral analysis of all three conditions (SI versus colon; GF versus SPF and ZT0 versus ZT12) revealed 16 GO terms to constitute common denominators that potentially represented diurnally adapting transcriptomic pathways that were specific to SI and modulated by time and the microbiome (Figure 1A). Among them were GO terms of circadian clock machinery, pathways responsible for absorption, intracellular transport, and antimicrobial defense. Surprisingly, several of the common denominator GO terms included pathways related to antigen processing and presentation via major histocompatibility complex (MHC) class II complex (Figure 1A). Indeed, SIECs were previously suggested to act as non-classic antigen-presenting cells that closely interact with lymphocyte populations of SI through MHC class II, thereby directing $CD4^{+}Foxp3^{+}$ T-regulatory cell differentiation (Westendorf et al., 2009), while reciprocally, T helper cell-derived cytokines have been reported to direct the development of MHC class II^{+} SI stem cells (Biton et al., 2018). Furthermore, SIEC MHC-class-II-mediated activity was shown to be induced by the gut microbiome and play a critical role in graft versus host disease (Koyama et al., 2019).

SIEC MHC Class II Expression Is Diurnally Regulated

We next examined the baseline frequency of MHC-class-II-expressing mature intestinal cells ($CD45^{-}$ $EpCAM^{HI}$) along the gastro-intestinal tract of *ad libitum* normal chow (NC)-fed 8-week-old male C57BL6 mice, at peak (ZT12) or trough (ZT0) time points (Figures 1B–1D, pooled results, three independent repeats). The frequency of MHC class II^{+} SIECs was significantly higher at ZT12 as compared to ZT0. In contrast to the SI, the cecum and colon showed no such temporal expression differences and a much lower MHC class II^{+} SIEC frequency. To exclude a vivarium-specific or a strain-specific effect, we further compared the frequency of MHC II^{+} SIECs between wild-type (WT) male, 8-week-old C57BL6 mice that were housed at our vivarium (Weizmann Institute of Science) for more than ten generations, to that of 8-week-old C57BL6 mice purchased from two independent commercial vendors (Jackson Laboratory, Figure S1D, and Envigo, Figure S1E), as well as to gender- and age-matched outbred Swiss Webster mice housed at our facility (Figure S1F). Indeed, the frequency of MHC class II^{+} SIECs exhibited a temporally shifting pattern across vivaria and genetic strains. These results suggested that a subpopulation of MHC class II^{+} SIEC may feature a diurnally regulated MHC class II expression profile.

Please cite this article in press as: Tuganbaev et al., Diet Diurnally Regulates Small Intestinal Microbiome-Epithelial-Immune Homeostasis and Enteritis, Cell (2020), https://doi.org/10.1016/j.cell.2020.08.027

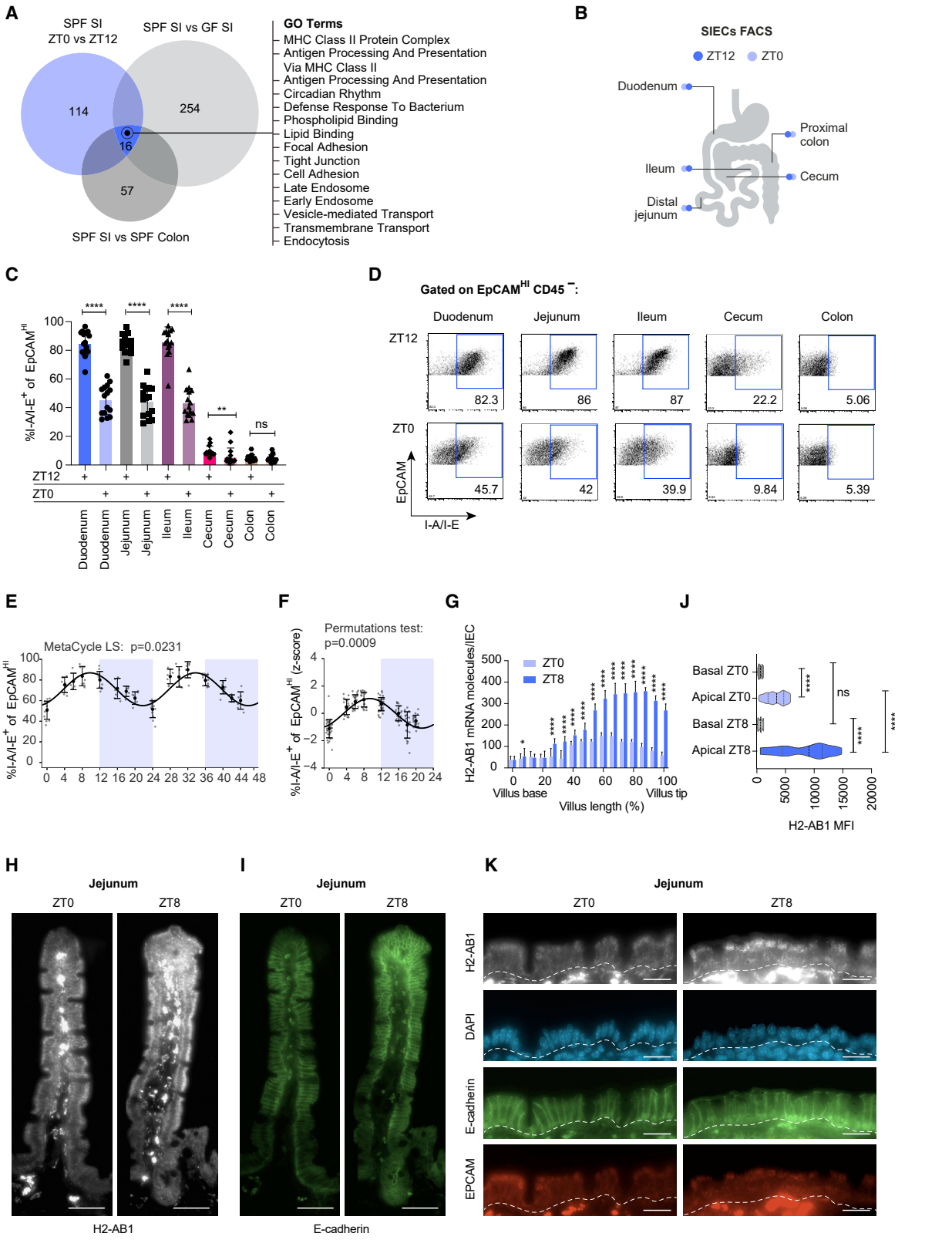

(legend on next page)

Please cite this article in press as: Tuganbaev et al., Diet Diurnally Regulates Small Intestinal Microbiome-Epithelial-Immune Homeostasis and Enteritis, Cell (2020), https://doi.org/10.1016/j.cell.2020.08.027

In vivo examination of the frequency of MHC class II$^+$ SIECs collected every 4 h throughout two consecutive 24-h cycles in male, 10-week-old C57BL6 mice confirmed that SIEC MHC class II protein expression features a diurnally oscillating pattern (meta cycle Lomb-Scargle [LS] p = 0.0231, Figure 1E, pooled results, four independent repeats; permutation test [PT] p = 0.0009, Figure 1F). Likewise, at the mRNA level, expression levels of a MHC class II representative gene H2-AB1 were highest at ZT4 and minimal at ZT20 and featured a diurnal pattern (LS p = 0.0438, PT p = 0.0009, Figures S1G and S1H). In contrast, SIEC expression of H1-K1 gene, a MHC class I member (Figures S1I and S1J, LS p = 0.9882; PT p = 0.1904), as well as that of interferon (IFN)-γ (Figures S2A and S2B, LS p = 0.8053; PT p = 0.2121), and EpCAM (protein level expression, Figures S2C and S2D, LS p = 0.9915; PT p = 0.5444; mRNA level expression, Figures S2E and S2F, LS p = 0.7460; PT p = 0.0766) did not exhibit diurnal oscillations. Overall, these results suggest that, in contrast to colonic IECs, EpCAM^{HI} SIECs express MHC class II at steady state, and a large subpopulation of SIECs exhibits diurnal patterns in levels of MHC class II expression on both protein and mRNA levels.

We next set out to spatially define the oscillating MHC class II$^+$ SIEC subpopulation, since SIEC subsets specialize in various tasks along a villus height, including anti-microbial defense at the bottom of the crypt, absorptive function at the middle of the villi, and immunomodulation at the top of the villi (Moor et al., 2018). Single-molecule fluorescence in situ hybridization (smFISH) performed at the trough (ZT0) and peak (ZT8) of SIEC MHC class II expression on the jejunum of WT male, 8-week-old C57BL6 mice demonstrated that the distribution of H2-AB1 mRNA is zonated along the length of villi in a time-specific manner. The highest concentration of mRNA molecules localized to the upper third of villi at ZT8, and to the middle of villi at ZT0 (Figures 1G and 1H), suggesting that the temporally oscillating SIEC MHC class II$^+$ population may be involved in nutrient absorption, which occurs within the same region at a similar time range (Moor et al., 2017; Moor et al., 2018), together with the peak of SI motility (Goo et al., 1987; Hoogerwerf et al., 2010; Kumar et al., 1986) and intestinal blood outflow to the liver (Lemmer and Nold, 1991). Interestingly, SIEC E-cadherin expression distribution mirrored that of H2-AB1 (Figure 1I; Figure S2G). Intracellularly, H2-AB1 mRNA molecules were concentrated at the apical side of SIECs (Figures 1J and 1K). Indeed, H2-AB1 was among the 30% most highly expressed polar localized mRNAs molecules within IECs (Moor et al., 2018), with higher mRNA concentration noted in the ribosome-enriched apical cell side, a subcellular locality previously suggested to allow IECs to rapidly respond to external stimuli such as food intake (Moor et al., 2017).

Dietary Composition and Feeding Rhythmicity Regulate SIEC MHC Class II Expression

Given the diurnal MHC class II activity noted in SIECs, we next set out to determine whether intact circadian clocks of the host are required for diurnal fluctuations of SIEC MHC class II expression. Toward this aim, we utilized both genetic and environmental models of circadian clock disruption to examine the SIEC MHC class II$^+$ population. The frequency of MHC class II$^+$ SIECs was examined every 6 h throughout two consecutive 24-h cycles in male, 8-week-old Period 1/2 double knockout (Per1/2 DKO) mice, which are deficient in core circadian clock genes and characterized by arrhythmic feeding (Bae et al., 2001), as compared to age- and gender-matched circadian clock-sufficient WT C57BL6 mice. Indeed, diurnal pattern of SIEC MHC class II expression was opposite in Per1/2 DKO mice compared to WT mice in both protein (Figures 2A and 2B, LS p = 0.1849; PT p = 0.0028, pooled results, two independent repeats; Figure S2H) and mRNA levels (Figures S2I and S2J, LS p = 0.147; PT p = 0.0013), with no diurnal changes noted in expression of the epithelial marker EpCAM (Figures S3A and S3B, LS p = 0.878; PT p = 0.6626). Similarly, examination of MHC class II$^+$ SIEC frequency in jet-lagged mice, subjected to 4 weeks of regular re-adaptation to an 8-h phase shift in light/dark cycle (Figure 2C), demonstrated a loss of diurnal pattern of SIEC MHC class II expression at ZT0 and ZT8 compared to control mice (Figure 2D, pooled results, three independent repeats).

As circadian clocks in mammals feature a hierarchical two-tier structure, featuring central hypothalamic circadian clocks and peripheral circadian clocks within each cell of the body, we next examined whether the diurnal MHC class II activity of SIECs requires endogenous SIEC clocks. Toward this aim, we generated intestinal epithelial specific knockout of Bmal1—a key member of circadian clock machinery, which featured an intact SIEC MHC class II protein expression at both trough (ZT0) and peak (ZT8) time points (Figure 2E, pooled results, three independent repeats). We next examined whether feeding rhythmicity might serve as the mechanism for the entrainment of diurnal SIEC MHC class II activity. Time-restricted feeding (TRF), limiting food access of 8-week-old WT and arrhythmic Per1/2 DKO male

Figure 1. SIEC MHC Class II Expression Undergoes Temporal and Biogeographical Diurnal Oscillations

(A) Venn diagram of shared and unique gene pathways in sorted SIECs comparing: SI germ-free versus SPF mice, SPF colon versus SI, and SPF SI at ZT0 versus ZT12. q < 0.1.

(B) Schematic showing sampling times and locations along the gastrointestinal tract for SIEC MHC class II fluorescence-activated cell sorting (FACS) analysis.

(C and D) Frequency of MHC class II$^+$CD45$^-$EpCAM^{hi} SIECs at ZT0 versus ZT12 across differential gastrointestinal regions.

(E and F) Frequency of MHC class II$^+$CD45$^-$EpCAM^{hi} SIECs over 48 h (E) or 24 h (F). Isolated SIECs from distal jejunum were examined every 4 h across two consecutive 24-h cycles. Data presented as sine curve fit and p values were calculated by LS test for 48 h (E) or by PT for 24 h (F).

(G) *H2-AB1* mRNA distribution alongside the length of villi in distal jejunum at ZT0 versus ZT8.

(H) Distribution of H2-AB1 mRNA alongside the length of villi from distal jejunum at ZT0 versus ZT8. Scale bar, 20 μm.

(I) Distribution of E-cadherin protein alongside the length of villi from distal jejunum at ZT0 versus ZT8. Scale bar, 20 μm.

(J) Mean fluorescence intensity of *H2-AB1* mRNA intracellular distribution in the distal jejunum at ZT0 versus ZT8.

(K) Intracellular distribution of *H2-AB1*, E-cadherin, and EPCAM in SIECs of distal jejunum at ZT0 versus ZT8. Dotted line highlights the borders between the epithelium and *lamina propria*.

Scale bar, 10 μm. *p < 0.05, **p < 0.01, ***p < 0.001, ****p < 0.0001 by Mann-Whitney U test; Figure 1G: 2-way ANOVA test. See also Figures S1 and S2.

Please cite this article in press as: Tuganbaev et al., Diet Diurnally Regulates Small Intestinal Microbiome-Epithelial-Immune Homeostasis and Enteritis, Cell (2020), https://doi.org/10.1016/j.cell.2020.08.027

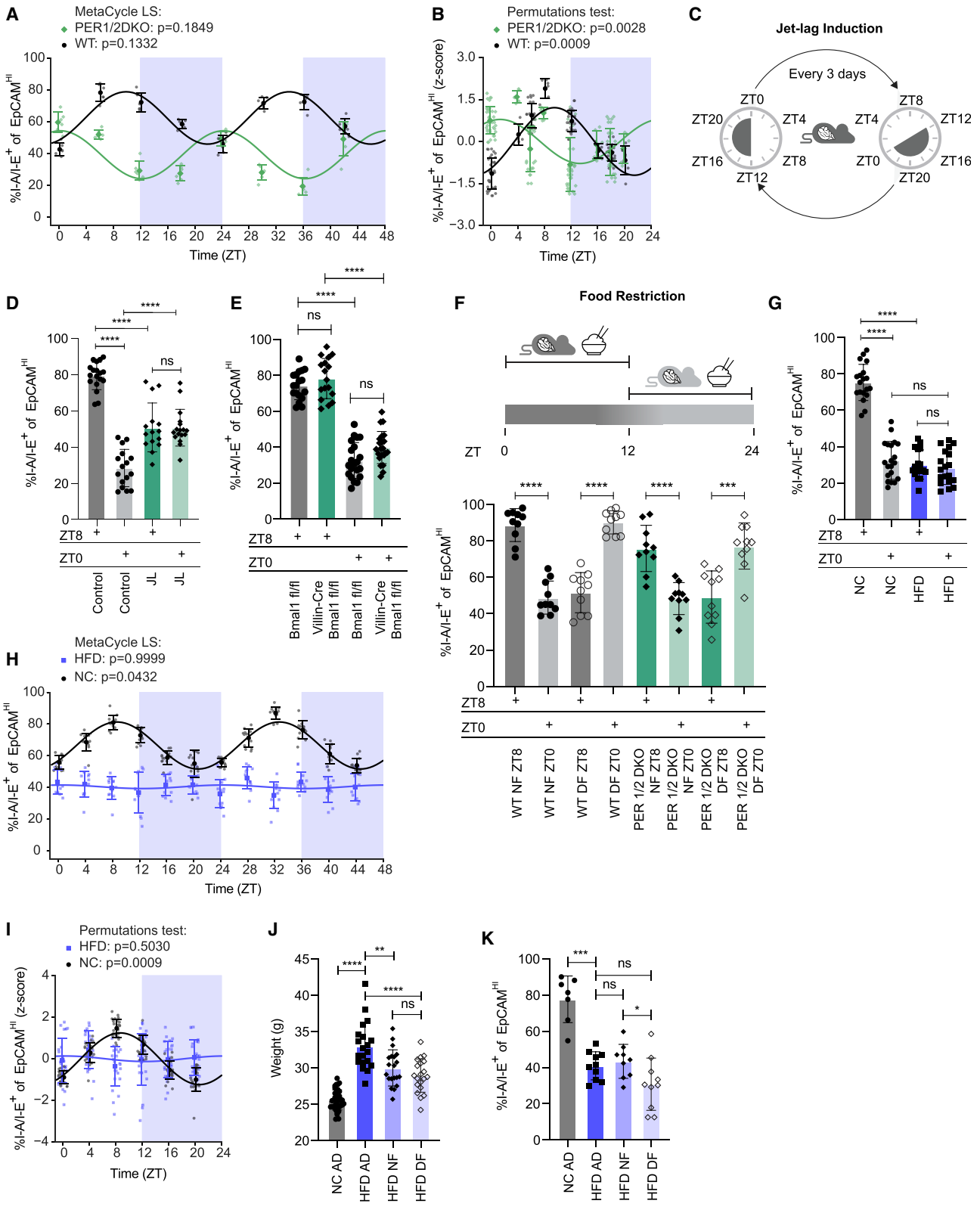

(legend on next page)

Please cite this article in press as: Tuganbaev et al., Diet Diurnally Regulates Small Intestinal Microbiome-Epithelial-Immune Homeostasis and Enteritis, Cell (2020), https://doi.org/10.1016/j.cell.2020.08.027

mice exclusively to the dark phase (night-fed group, NF) or to the light phase (day-fed group, DF) of a 24-h cycle for 4 weeks, uncovered a feeding-dependent phase-shift in diurnal MHC class II expression in WT mice, and a restored rhythmic SIEC MHC class II expression in Per1/2 DKO mice (Figure 2F, pooled results, two independent repeats). These results suggested that feeding rhythmicity may contribute to diurnal rhythmicity entrainment of SIEC MHC class II expression.

To uncover whether compositional dietary alterations, complementary to the above temporal dietary cues, may shape the diurnal expression pattern of SIEC MHC class II, we determined the *in vivo* SIEC MHC class II expression pattern in C57BL6, male 12-week-old mice fed *ad libitum* high-fat diet (HFD), containing 60% of calories in fat versus NC for 4 weeks at ZT0 and ZT8. Indeed, a dietary switch from NC to HFD led to a marked reduction on the protein frequency of MHC class II$^+$ SIECs at ZT8 to ZT0 levels (Figure 2G, pooled results, four independent repeats). Likewise, a repetitive 4-h measurement of MHC class II expression throughout a 48-h period upon transition to HFD demonstrated an overall reduction of SIEC MHC class II expression and a loss of the diurnal pattern on both protein (Figures 2H and 2I, HFD LS p = 0.9999; PT p = 0.5030 pooled results, two independent repeats) and mRNA levels (Figures S3C and S3D, HFD LS p = 0.5584; PT p = 0.2679), with no changes noted in expression of the epithelial marker EpCAM (Figures S3E and S3F, HFD LS p = 0.8519; PT p = 0.5887). To dissociate indirect effects of HFD on diurnal MHC class II expression mediated by its impact on the timing of feeding in mice, from its direct effects on rhythmic MHC class II expression, we applied time-restricted feeding (TRF) to HFD-fed mice (Figures 2J and 2K). While TRF induced weight loss (Figure 2J), it did not reverse the HFD-mediated suppression of SIEC MHC class II expression (Figure 2K), suggesting that the effects of HFD on SIEC MHC class II can be predominantly attributed to its dietary composition rather than its indirect effects on feeding behavior. Collectively, these results suggest that feeding rhythmicity and dietary content both act as regulators of diurnal SIEC MHC class II expression.

Dietary Regulation of SIEC MHC Class II Expression Is Dependent on the Microbiome

We next sought to decode the mechanism by which dietary interventions modulate SIEC MHC class II expression. One such mechanism may include regulation by the intestinal microbiome (Thaiss et al., 2015, 2016). Indeed, we found that, similarly to large intestinal community (Thaiss et al., 2014), the SI microbiome undergoes time-of-day-specific changes in its composition, both in the lumen (Figures S3G and S3I) and mucosal fraction (Figures S3H and S3J). To test whether the SI microbiome participates in regulation of SIEC MHC class II, we examined diurnally shifting SIEC MHC class II expression under microbiome disruptive conditions, in either 12-week-old C57BL6 male GF mice or gender-and age-matched mice treated with a broad-spectrum antibiotics cocktail consisting of ampicillin, vancomycin, metronidazole, and neomycin (AVMN) in drinking water for 4 weeks. In both conditions, the frequency of MHC class II$^+$ SIECs was reduced, and the diurnal pattern of expression lost, as compared to non-microbiome-disrupted controls (Figure 3A, pooled results, two independent repeats; Figure S4A). To corroborate these findings, we examined SIEC MHC class II expression every 4 h throughout two consecutive 24-h cycles in 12-week-old GF male mice and in age- and gender-matched AVMN-treated male mice compared to non-microbiome-disrupted controls. While control SPF mice exhibited a SIEC MHC class II diurnal pattern (LS p = 0.0496; PT p = 0.0009), GF mice (LS p = 0.9574; PT p = 0.7474) and AVMN-treated mice (LS p = 0.3578; PT p = 0.1730) featured a reduced MHC class II$^+$ SIECs frequency and an absent diurnal pattern of expression on both protein (Figures 3B and 3C, pooled results, two independent repeats) and mRNA levels (Figures S4B and S4C).

To further delineate the microbiome members involved in SIEC MHC class II induction, we examined SIEC MHC class II expression in 12-week-old C57BL6 male mice treated for 4 weeks with individual components of the AVMN broad-spectrum antibiotics regimen. Importantly, vancomycin treatment, but none of the other three antibiotics, induced a substantial decrease in MHC class II$^+$ SIEC frequency (Figure 3D, pooled results, three independent repeats), suggesting that gram-positive vancomycin-sensitive bacteria may drive SIEC MHC class II expression at our vivarium. In agreement, mice treated for 4 weeks with metronidazole retained a diurnal pattern of SIEC MHC class II expression at ZT8 versus ZT0, while this pattern was lost upon vancomycin treatment (Figure 3E, pooled results, three independent repeats). To further prove that the microbiome directly impacts SIEC MHC class II expression, we transferred microbiomes

Figure 2. SIEC MHC Class II Diurnal Oscillations Are Regulated through Diet Composition and Rhythmicity

(A and B) Frequency of MHC class II$^+$CD45$^-$EpCAM^{hi} SIECs across 48 h (A) and summarized for two consecutive 24 h (B) in Per1/2 DKO mice versus control mice. Data presented as sine curve fit and p values were calculated by LS test for 48 h (A) or by PT for 24 h (B).

(C) Schematic illustrating model of chronic environmental circadian cycle disruption (jet lag) in which mice are subjected to an 8-h shift in light/dark cycle every 3 days for 4 weeks.

(D) Frequency of MHC class II$^+$CD45$^-$EpCAM^{hi} SIECs at distal jejunum of jet-lagged mice versus controls at ZT0 versus ZT8.

(E) Frequency of MHC class II$^+$CD45$^-$EpCAM^{hi} SIECs at distal jejunum of Villin-cre Bmal1 fl/fl mice versus Bmal fl/fl littermate controls at ZT0 versus ZT8.

(F) Frequency of MHC class II$^+$CD45$^-$EpCAM^{hi} SIECs at distal jejunum of mice of WT or PER1/2 DKO mice that were either day or night fed (DF or NF, respectively) at ZT0 versus ZT8.

(G) Frequency of MHC class II$^+$CD45$^-$EpCAM^{hi} SIECs at distal jejunum of mice fed with NC versus HFD at ZT0 versus ZT8.

(H and I) Frequency of MHC class II$^+$CD45$^-$EpCAM^{hi} SIECs at distal jejunum of mice fed with NC versus HFD across 48 h (H) and summarized for two consecutive 24-h periods (I). Data presented as sine curve fit and p values were calculated by LS test for 48 h (H) or by PT for 24 h (I).

(J) Body weight of WT mice fed with NC, HFD *ad libitum* (AD), and HFD day or night fed (HFD DF or HFD NF, respectively).

(K) Frequency of MHC class II$^+$CD45$^-$EpCAM^{hi} SIECs at distal jejunum of mice of WT mice fed with NC, HFD AD, and HFD day or night fed (HFD DF or HFD NF, respectively). All data represent at least two independent experiments.

Means ± SD are plotted. *p < 0.05, **p < 0.01, ***p < 0.001, ****p < 0.0001 by Mann-Whitney U test. See also Figures S2 and S3.

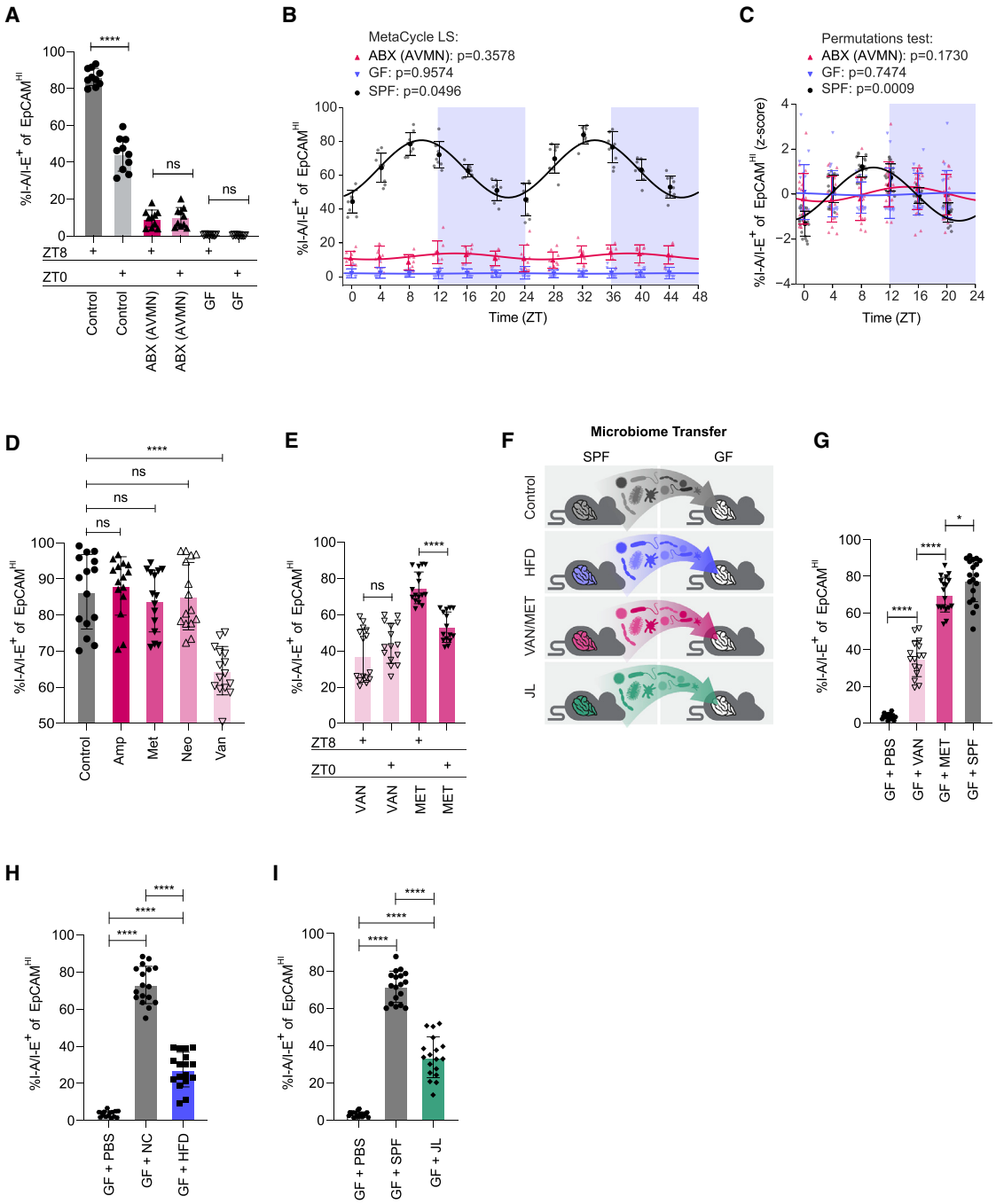

Figure 3. Dietary Modulation of SIEC MHC Class II Is Mediated by SI Microbiome

(A) Frequency of MHC class II^{+}CD45^{-}EpCAM^{hi} SIECs at distal jejunum of control mice versus AVMN antibiotic cocktail-treated and germ-free (GF) mice at ZT0 versus ZT8.

(B and C) Frequency of MHC class II^{+}CD45^{-}EpCAM^{hi} SIECs from distal jejunum of control mice versus antibiotics-treated mice (ABX) or germ-free mice (GF) examined every 4 h across 48 h (B) and average of two consecutive 24 h (C). The line represents the sine fit curve, and p values were calculated by LS test for 48 h (B) or by PT for 24 h (C).

(D) Frequency of MHC class II^{+}CD45^{-}EpCAM^{hi} SIECs at distal jejunum of mice treated with ampicillin (AMP), vancomycin (VAN), metronidazole (MET), or neomycin (NEO) examined at ZT8.

(E) Frequency of MHC class II^{+}CD45^{-}EpCAM^{hi} SIECs at distal jejunum of mice treated with vancomycin (VAN) or metronidazole (MET) at ZT0 versus ZT8.

(F) Schematic illustrating reconstitution of recipient germ-free (GF) mice with luminal microbiome transfer from the distal jejunum of HFD-fed specific pathogen-free (SPF), SPF mice treated with vancomycin (VAN) or metronidazole (MET), or SPF mice subjected to chronic jet lag (JL).

(legend continued on next page)

Please cite this article in press as: Tuganbaev et al., Diet Diurnally Regulates Small Intestinal Microbiome-Epithelial-Immune Homeostasis and Enteritis, Cell (2020), https://doi.org/10.1016/j.cell.2020.08.027

from either metronidazole or vancomycin-treated mice into 8-week-old C57BL6 GF male mice (Figures 3F and 3G, pooled results, three independent repeats) and examined, 2 weeks later, SIEC MHC class II expression in recipient mice. While microbiomes from metronidazole-treated mice successfully induced SPF control levels of SIEC MHC class II expression, microbiomes from vancomycin-treated mice failed to induce such levels of SIEC MHC class II, suggesting that the vancomycin-impacted microbiome is deficient in its SIEC MHC-class-II-inducing capacity for at least 2 weeks after antibiotic exposure.

Having separately linked either the gut microbiome or diet as regulators of SIEC MHC class II expression, we set out to explore whether the observed dietary effect on MHC class II$^+$ SIEC frequency acts upstream to the microbiome. To this aim, we transferred microbiomes from either HFD or NC *ad libitum* fed male mice into 8-week-old C57BL6 GF male mice and examined, 2 weeks later, MHC class II$^+$ SIEC frequency (Figures 3F and 3H, pooled results, three independent repeats) in recipient mice. While the microbiome from NC-fed mice induced a high SIEC MHC class II expression, the microbiome from HFD-fed donors failed to do so, demonstrating that the effect of HFD on SIEC MHC class II expression is mediated, at least partially, by the microbiome. However, while the HFD microbiome induced low SIEC MHC class II expression, it remained significantly higher than the GF baseline SIEC MHC class II expression level, suggesting that some commensals in the HFD microbiome configuration retain an ability to induce low and temporally stable level SIEC MHC class II expression. Concordantly, "low" SIEC MHC class II expression of 16-week-old C57BL6 HFD-fed male mice could be further inhibited by the AVMN antibiotic regimen (Figures S4D and S4E). To further explore whether the observed effect of circadian clock disruption on SIEC MHC class II expression is mediated through dietary impacts on the microbiome, we transferred the microbiome from 12-week-old C57BL6 jet-lagged or control mice into 8-week-old C57BL6 GF male mice (Figures 3F and 3I, pooled results, three independent repeats) and examined, 2 weeks later, SIEC MHC class II expression in recipient mice. Indeed, the microbiome from jet-lagged mice failed to induce SIEC MHC class II expression, thereby demonstrating that the effect of circadian clock disruption on SIEC MHC class II population is mediated, at least partially, by the microbiome. Together, these results suggest that the SI microbiome serves as a signaling hub integrating dietary composition and timing inputs and entrains diurnality of MHC class II expression in SIECs.

Distinct Small Intestinal Commensals Induce SIEC MHC Class II Expression through Contact-Dependent Mechanisms

We next sought to identify which members of the SI microbiome orchestrate diurnal regulation of the MHC class II$^+$ SIEC population at our vivarium. To this aim, we examined SI luminal and mucosal microbiome compositions under the conditions featuring low SIEC MHC class II expression, namely, treatment of 12-week-old C57BL6 male mice with vancomycin (Figures S4F–S4I), or exposure to HFD (Figure S4J). Overall, we identified 6 bacterial taxa (*Lactobacillus*, *Sutterella*, *Curtobacterium*, *Parabacteroides*, *Desulfovibrio*, *Aggregatibacter*) to be enriched at the SI mucosa in conditions characterized by low SIEC MHC class II expression (HFD and vancomycin), while 9 bacterial taxa (*Coprococcus*, *Ruminococcus*, *Allobaculum*, *Akkermansia*, *Candidatus Arthromitus*, *Streptococcus*, *Oscillospira*, *Dorea*, *Christensenella*) were over-represented when SIEC MHC class II expression was high (NC, metronidazole, Table S1). To further pinpoint potential SIEC MHC class II modulators, we treated 8-week-old C57BL6 male mice with either metronidazole, vancomycin, or their combination, to induce a reduction in SIEC MHC class II expression upon vancomycin exposure, followed by a 2-week recovery period in which SIEC MHC class II expression concomitantly returned to control levels (Figures 4A and 4B, pooled results, two independent repeats). SI microbiome 16S rDNA composition and SIEC MHC class II protein expression were concomitantly assessed at baseline, after completion of antibiotic intervention, and at the time of reversion of SIEC MHC class II to baseline levels. Cross-correlation analysis identified 3 potential "inducers" (*Candidatus Arthromitus*, *Lachnospiraceae*, *Akkermansia*) and 5 potential "suppressors" (*Lactobacillus*, *Sutterella*, *Erwinia*, *Allobaculum*, *Ruminococcus*) at our vivarium, whose relative abundance positively or negatively correlated with all phases of changes of SIEC MHC class II expression (Figure 4C). As this culture-independent search may be susceptible to PCR bias toward more abundant species (Lau et al., 2016), we complemented it with "culturomics" analysis of SI mucosal microbiome samples from metronidazole- or vancomycin-treated mice (Figure 4D) by growing them aerobically or anaerobically on 31 types of media (Lau et al., 2016). 16S rDNA analysis of grown colonies (Figure 4D) identified a list of 3 potential "inducers" (*Erwinia*, Lachnospiraceae, *Akkermansia*) and 7 potential "suppressors" (Lactobacillaceae, *Pseudomonas*, *Streptococcus*, *Ruminococcus*, *Allobaculum*, Helicobacteraceae, Chromatiaceae) of SIEC MHC class II expression that could be isolated from mice *in vivo*. Importantly, results of the culturomics approach were mostly consistent with those of the culture-independent approach.

In order to directly test the predicted associations between the SIEC MHC class II and potential "inducers" and "suppressors," we then mono-colonized 8-week-old C57BL6 GF male mice for 2 weeks with predicted "inducers" and one of the predicted "suppressors" as compared to heat-inactivated strains. Indeed, we demonstrated that live "inducers" such as *Akkermansia* (AKK), Lachnospiraceae (LH), and segmented filamentous bacteria (SFB) induced SIEC MHC class II expression, while the live predicted "suppressor" *Lactobacillus Murinus* (LBM) as well as heat-inactivated "inducers" failed to do so (Figures 4E and 4F; Figure S5A). As the "inducer" genera *Akkermansia*, Lachnospiraceae and SFB belong to a group of mucosa-associated bacteria that actively attach to the SIECs as part of their natural behavior, we determined whether attachment to SIECs by an inducer strain

(G–I) Frequency of MHC class II$^+$CD45$^-$EpCAM^{hi} SIECs at distal jejunum of ex-GF mice reconstituted with luminal microbiome from the distal jejunum of either mice treated with vancomycin (VAN) or metronidazole (MET) compared to SPF mice (G), mice fed HFD versus NC (H), and mice subjected to chronic jet lag (JL) (I) compared to control donor mice. All data represent at least two independent experiments.
Means ± SD are plotted. *p < 0.05, **p < 0.01, ***p < 0.001, ****p < 0.0001 by Mann-Whitney U test. See also Figures S3 and S4 and Table S1.

Please cite this article in press as: Tuganbaev et al., Diet Diurnally Regulates Small Intestinal Microbiome-Epithelial-Immune Homeostasis and Enteritis, Cell (2020), https://doi.org/10.1016/j.cell.2020.08.027

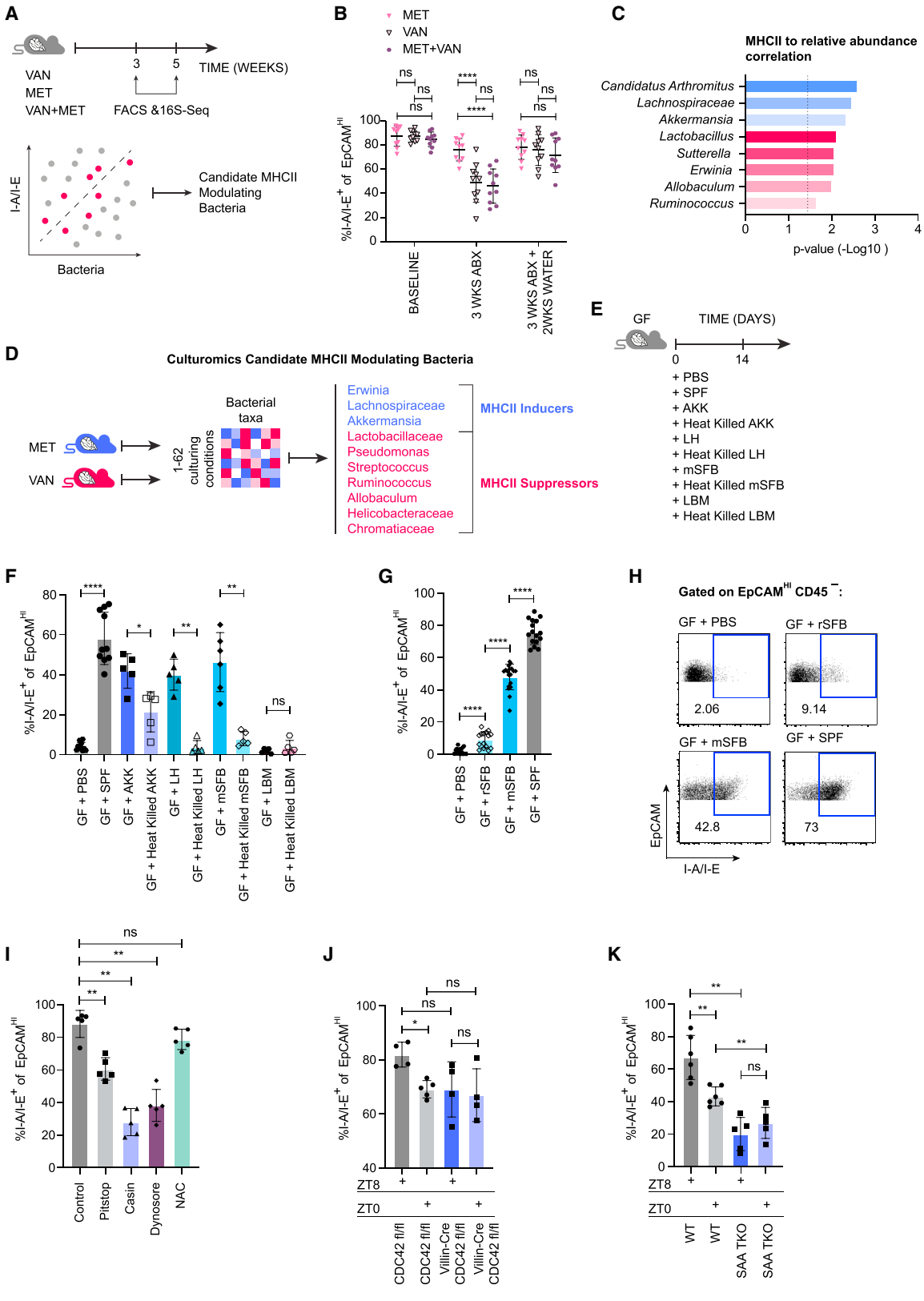

(legend on next page)

Please cite this article in press as: Tuganbaev et al., Diet Diurnally Regulates Small Intestinal Microbiome-Epithelial-Immune Homeostasis and Enteritis, Cell (2020), https://doi.org/10.1016/j.cell.2020.08.027

is important for the induction of MHC class II expression. Toward this aim, we mono-colonized 8-week-old C57BL6 GF male mice with either mouse SFB (mSFB) or rat SFB (rSFB), with only the former being able to effectively colonize the mouse SI mucosa (Atarashi et al., 2015; Thaiss et al., 2016). Indeed, only mSFB was able to induce SIEC MHC class II expression in GF mice, while rSFB failed to do so, indicating that epithelial attachment may be required for the induction of SIEC MHC class II expression by mSFB (Figures 4G and 4H, pooled results, three independent repeats). We next sought to determine whether previously described mechanisms downstream of SFB attachment to IECs, namely, CDC42-mediated microbial adhesion triggered endocytosis (MATE) (Ladinsky et al., 2019) and Serum Amyloid A (SAA)-mediated signaling (Atarashi et al., 2015), modulate SIEC MHC class II expression. Indeed, chemical inhibition of several endocytosis pathways in SIECs (Figure 4I) suggested that CDC42-dependent, clathrin-independent, dynamin-dependent endocytosis contributed to regulation of SIEC MHC class II expression. Similarly, the absence of epithelial CDC42 resulted in the loss of diurnal pattern in SIEC MHC class II expression (Figure 4J). Moreover, mucosal SI microbiome of Villin-Cre-CDC42$^{fl/fl}$ mice was depleted of MHC class II inducer bacteria, such as SFB and *Akkermansia*, akin of other SIEC MHC class II disruptive conditions (Figure S5B), while whole body deletion of SAA genes 1, 2, and 3 (SAA triple-knockout mice) was associated with an absence of SIEC MHC class II diurnal activity as compared to co-housed controls (Figure 4K). Collectively, these results suggest that rhythmic feeding entrains distinct diurnal SI commensals, which, in turn, induce diurnal fluctuation of SIEC MHC class II through the CDC42 and SAA pathways. Disruption of homeostatic SI microbiome composition by dietary changes (HFD) or antibiotic perturbation leads to depletion of SIEC MHC-class-II-inducing microbial species.

SIEC MHC Class II Expression Supports Diurnal Activity of Intra-epithelial T Cell IL-10$^+$ Lymphocytes

We next aimed to uncover downstream impacts of diet and microbiome-regulated SIEC MHC class II expression on SIEC immunity. To this aim, we generated conditional knockout mice lacking a functional beta chain of the MHC class II complex (I-Ab) (Hashimoto et al., 2002) specifically in mature enterocytes (Villin-Cre-I-Ab$^{fl/fl}$, Figures S5C–S5E) and explored MHC class II contribution to interactions of SIECs with SI intra-epithelial lymphocytes (IELs), as was previously described in the large intestine (Biton et al., 2018; Westendorf et al., 2009). Surprisingly, we found that 8-week old Villin-Cre I-Ab$^{fl/fl}$ mice featured a significant reduction in the frequency of CD4$^+$ T IELs (Figure 5A, pooled results, three independent repeats) as compared to littermate controls, suggesting that SIEC MHC class II is required for the SI IEL homeostasis. Furthermore, SIECs in Villin-Cre I-Ab$^{fl/fl}$Rag1$^{-/-}$ mice, adoptively transferred with 0.5 × 10^6 OVA-specific (OTII) T cells, failed to induce CD4$^+$ IEL proliferation following systemic introduction of an OVA antigen (Figure 5B). In contrast to MHC-class-II-expressing SIECs, "professional" antigen-presenting subpopulations and lamina propria CD4$^+$ lymphocytes remained unaltered in frequency in WT mice upon induction of HFD, a SIEC MHC-class-II-suppressing condition (Figures S5F–S5J). The SIEC-IEL MHC-class-II-mediated interaction seems to be unidirectional, as no difference in SIEC MHC class II was observed in CD4$^{-/-}$ mice comparing to littermate WT controls (Figure 5C) as well as in Rag1$^{-/-}$ mice lacking the adaptive immune arm (Figure S5K). In support of the SIEC MHC class II role in modulating homeostasis of the CD4$^+$ IEL population, conditions featuring impaired SIEC MHC class II expression, such as administration of vancomycin, but not ampicillin, neomycin, or metronidazole treatment, were associated with a diminished IEL CD4$^+$ T cell population (Figure 5D, pooled results, three independent repeats; Figure 5G). Similarly, GF mice reconstituted with microbiome from HFD-fed donors failed to increase their IEL CD4$^+$ T cell population compared to NC-microbiome-transferred GF mice (Figure 5E, pooled results, three independent repeats; Figure 5G), while GF mice mono-colonized with mSFB, but not with rSFB, featured an increase in their IEL CD4$^+$ T cell population (Figures 5F and 5G, pooled results, three independent repeats). Together, these findings indicate that SIEC MHC class II expression is linked to SI IEL expansion, while genetic or environmentally induced ablation of SIEC MHC class II expression leads to a diminished presence of SI IELs.

As several SI IEL populations, such as CD4$^+$ CD8β$^-$FOXP3$^+$ IL-4$^-$ cells, were previously shown to play an immune-tolerogenic role mediated in part through IL-10 secretion (Carton et al., 2004; Das et al., 2003; McDonald et al., 2018; Senju et al.,

Figure 4. SI Microbiome Induces SIEC MHC Class II through Diurnal Attachment

(A) Schematic illustration of experimental design.

(B) Frequency of MHC class II$^+$CD45$^-$EpCAM^{hi} SIECs at distal jejunum of mice treated with vancomycin (VAN), metronidazole (MET), or their combination (VAN+MET) followed by a treatment switch in all groups to water. The frequency was assessed at baseline, at the end of antibiotic treatment and after the recovery period.

(C) Abundance of luminal SI bacterial taxa that were significantly correlated to MHC class II$^+$CD45$^-$EpCAM^{hi} SIECs (Meta_Cycle $p < 0.05$ and $q < 0.1$).

(D) Significantly variable bacterial taxa between the luminal distal jejunum microbiome of vancomycin (VAN) versus metronidazole (MET)-treated mice based on culturomics experiments. Highlighted are the candidate SIEC MHC class II suppressors (red) and inducers (blue) taxa confirmed by an intervention experiment (E and F). Significance: ($q < 0.1$) Wilcoxon rank-sum with FDR correction.

(E and F) Schematic illustrating the intervention experimental design (E) and frequency of MHC class II$^+$CD45$^-$EpCAM^{hi} SIECs (F) of germ-free (GF) mice mono-colonized with bacteria based on the culturomics results composition (16S-rDNA Sequencing).

(G and H) Frequency of MHC class II$^+$CD45$^-$EpCAM^{hi} SIECs at distal jejunum (G) and and representative FACS plots (H) of germ-free (GF) mice reconstituted with distal jejunum microbiome from control SPF mice or mono-colonized with mouse or rat segmented filamentous bacteria (mSFB and rSFB, respectively).

(I) Frequency of MHC class II$^+$CD45$^-$EpCAM^{hi} SIECs at distal jejunum in mice treated with inhibitors of several endocytosis pathways.

(J and K) MHC class II$^+$CD45$^-$EpCAM^{hi} SIECs frequency in mice with epithelial deficiency of CDC42 (J) or in SAA triple-knockout mice (K) at ZT0 versus ZT8.

All data represent at least two independent experiments. Means ± SD are plotted. *$p < 0.05$, **$p < 0.01$, ***$p < 0.001$, ****$p < 0.0001$ by Mann-Whitney U test, Figure 4B: 2-way ANOVA test. See also Figures S4 and S5.

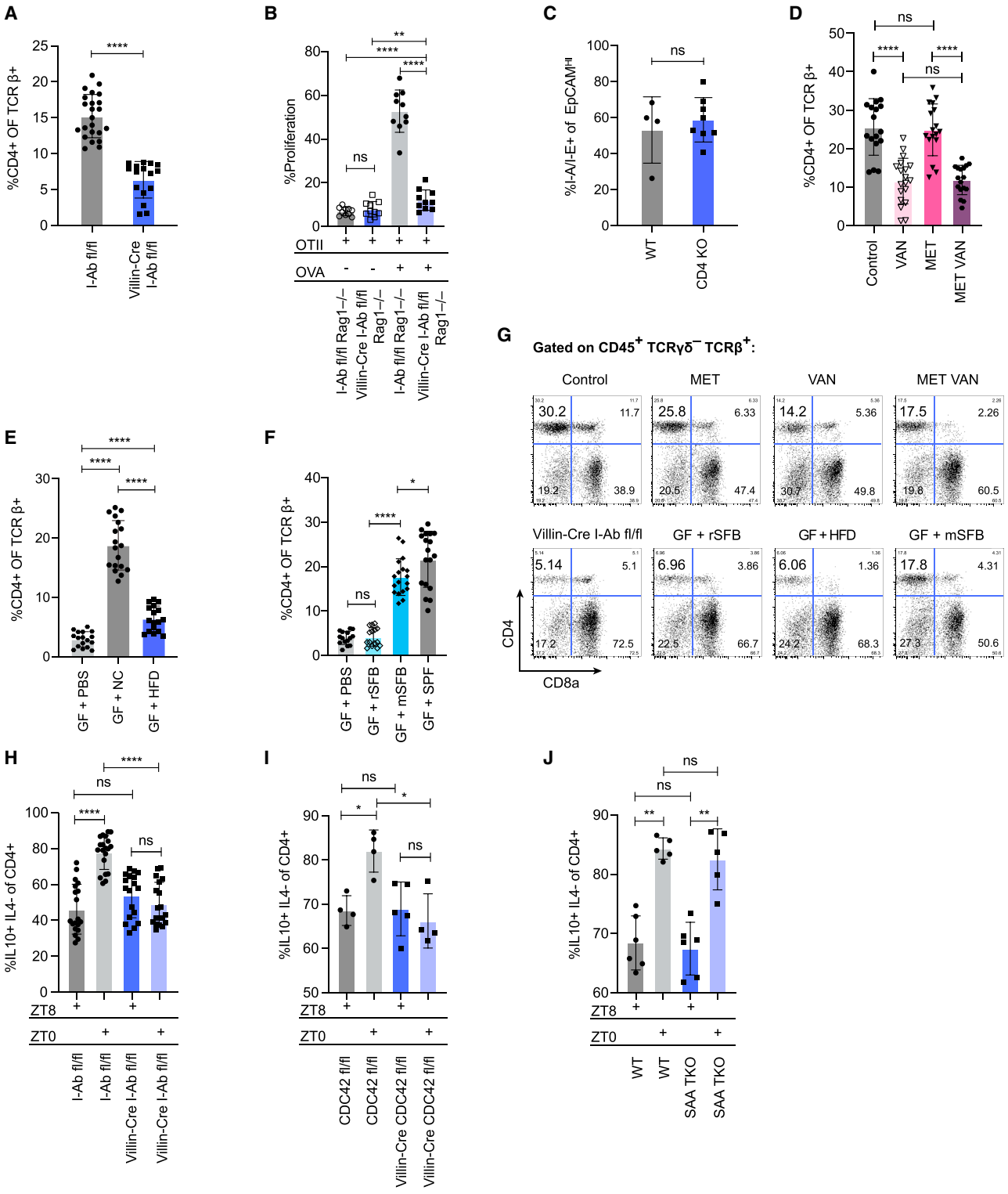

Figure 5. SIEC MHC Class II Shapes Diurnal Tolerogenic Activity of CD4$^+$CD8a$^-$TCR-αβ$^+$TCR-γδ$^-$Foxp3$^-$IL-4$^-$IL-10$^+$ IELs

(A) Frequency of SI CD4$^+$CD8a$^-$TCR-αβ$^+$TCR-γδ$^-$ intraepithelial lymphocytes in Villin-Cre MHC class II$^{flox/flox}$ (Villin-cre I-Ab fl/fl) mice versus MHC class II$^{flox/flox}$ (I-Ab fl/fl) littermates.

(B) Proliferation of adoptively transferred OTII CD4$^+$ T cells (OTII) in Villin-cre I-Ab fl/fl Rag1$^{-/-}$ versus I-Ab fl/fl Rag1$^{-/-}$ mice upon oral administration of ovalbumin (OVA).

(legend continued on next page)

Please cite this article in press as: Tuganbaev et al., Diet Diurnally Regulates Small Intestinal Microbiome-Epithelial-Immune Homeostasis and Enteritis, Cell (2020), https://doi.org/10.1016/j.cell.2020.08.027

1991; Sujino et al., 2016), we next investigated potential effects of SI MHC class II on SI IEL IL-10 protein expression at peak and trough of SI MHC class II expression in either Villin-Cre I-Ab$^{fl/fl}$ mice or littermate controls. *In vivo*, SI CD4 IEL IL-10 protein expression in WT I-Ab$^{fl/fl}$ littermates was significantly elevated at ZT0 compared to ZT8, while this diurnal shift in IL-10 protein expression was lost in Villin-Cre I-Ab$^{fl/fl}$ mice (Figure 5H, pooled results, three independent repeats). These results were corroborated by measurements of CD4$^+$ IEL-derived IL-10 levels every 6 h throughout a 24-h cycle (Figures S6A–S6C), in which IEL-derived IL-10 levels featured a diurnal pattern in untreated SPF WT C57BL6 control mice (Figure S6B, PT p = 0.0026) but not in broad-spectrum antibiotic (AVMN)-treated mice. Concordantly, environmental disruption of circadian clocks in a model of chronic jet lag negated diurnal fluctuations of SI CD4$^+$ IEL population frequency (Figures S6D–S6F). In support of the hypothesis that SIEC MHC class II expression is located downstream to mucosal bacterial attachment, we did not detect statistically significant differences in the mucosal microbiome of 8-week-old, male Villin-Cre I-Ab$^{fl/fl}$ mice versus I-Ab$^{fl/fl}$ littermates (Figure S6G). SI CD4$^+$ IEL IL-10 protein expression in Villin-Cre CDC42 $^{fl/fl}$ mice was similar between ZT8 and ZT0 (Figure 5I), reflecting a potential role of CDC42 in regulating SIEC diurnal control of downstream mucosal immunity. In contrast, SI CD4$^+$ IEL IL-10 protein expression in SAA TKO mice maintained its differences between ZT8 and ZT0, similar to WT controls (Figure 5J). Collectively, these results suggest CDC42 may be required, while SAA1, 2, and 3 are dispensable, for the diurnal production of IL-10 by SI CD4$^+$ IELs.

SIEC MHC Class II and Downstream IEL-Derived IL-10 Diurnally Regulate the SI Barrier Function

We next explored the physiological consequences of diurnal SIEC MHC-class-II-induced IL-10 expression on downstream SI function. One of the well-established roles of IEL-derived IL-10 is regulation of gut permeability, also termed barrier function (Carton et al., 2004; Das et al., 2003; McDonald et al., 2018; Senju et al., 1991; Sujino et al., 2016). To determine whether this physiologically critical function is diurnally regulated at steady state, we first examined SI ion permeability and transepithelial resistance every 4 h throughout two consecutive 24-h cycles (Figure S6H) and found both measures of gut barrier function to exhibit diurnal fluctuations (Figures 6A and 6B for ion permeability, LS p = 0.0717; PT p = 0.0009; pooled results, two independent repeats; Figures S6I–S6J for resistance, LS p = 0.0587; PT p = 0.0010). Importantly, the presence of an intact intestinal microbiome was necessary to support this homeostatic diurnal barrier function and was diminished by 4 weeks of broad-spectrum antibiotic (AVMN) treatment (Figures 6A and 6B for ion permeability, ABX (AVMN): LS p = 0.9999; PT p = 0.5888; pooled results, two independent repeats; Figures S6I and S6J for resistance, ABX (AVMN): LS p = 0.9999; PT p = 0.5416). We corroborated these barrier diurnal fluctuations by oral administration of fluorescein isothiocyanate (FITC)-coated 4 kDa dextran beads to mice at different time points across a 24 h period. This enabled generation of a time course quantification of barrier function (reflected by FITC MFI of peripheral blood samples) across the course of a 24 h period. Indeed, results suggested a diurnal pattern of SI permeability (Figure S6K, PT p = 0.0035). Similarly, quantification of pattern recognition receptors (PRRs) ligand concentrations (Thaiss et al., 2018) in the portal vein (Figure 6C), peripheral blood (Figure S6L), and the liver (Figure S6M) demonstrated a diurnal fluctuation of barrier function. Dietary rhythmicity was a potent regulator of diurnal SI barrier function. Disruption of circadian clocks by both genetic (Per1/2 deficiency) and environmental (chronic jet lag) perturbations led to a significant disruption in SI barrier function, as featured in SI ion permeability, epithelial resistance, FITC-dextran systemic influx and (PRR) ligand concentrations (Figure 6D, pooled results, three independent repeats; Figure S6N; Figure S7A). These effects were mediated by circadian modulation of feeding rhythmicity, as restoration of periodic feeding rhythmicity in Per1/2 DKO mice by TRF either during the light (day fed, [DF]) or dark phase (night fed [NF]) reversed the altered diurnal pattern of the SI barrier function in these mice (Figures S7B and S7C). Similarly, feeding-time restriction could shift the temporal dynamics of SI permeability in WT controls by 12 h (Figure 6E, pooled results, independent repeats; Figure S7D).

Dietary content was also a regulator of the SI barrier function, as HFD feeding of 12-week-old C57BL6 males impaired SI permeability, as featured in SI ion permeability, epithelial resistance, FITC-dextran systemic influx, and PRR ligand concentrations (Figure 6F, pooled results, three independent repeats**;** Figures S7E and S7F). Expectedly, TRF of HFD-fed 12-week-old C57BL6 male mice, either during the light or dark phases, had no effect on SI barrier function (Figures S7G–S7I). This dietary effect was driven by the HFD-induced altered microbiome, as fecal transplantation of microbiome from HFD-fed donors into GF mice significantly impaired SI permeability, as compared to recipients of microbiome from NC-consuming donors (Figure 6G, pooled results, three independent repeats; Figure S7J). SIEC MHC class II expression downstream of diet composition, feeding rhythms, and the associated SI microbiome likewise was demonstrated to regulate the SI barrier function, as Villin-Cre I-Ab$^{fl/fl}$ mice featured a 3-fold increase in gut permeability and loss of the diurnal pattern, compared to I-Ab$^{fl/fl}$ littermate controls (Figure 6H, pooled results, three independent repeats; Figures S7K and S7L). Systemic supplementation of

(C) Frequency of MHC class II$^+$CD45$^-$EpCAM^{HI} SIECs at distal jejunum in CD4$^{-/-}$ versus WT mice.
(D–G) Frequency (D–F) and representative FACS plot (G) of SI CD4$^+$CD8α^-TCR-$\alpha\beta^+$TCR-$\gamma\delta^-$ intraepithelial lymphocytes of (D) mice treated with vancomycin (VAN), metronidazole (MET), or their combination (VAN+MET), (E) germ-free (GF) mice reconstituted with luminal SI microbiome of HFD-fed mice (GF+HFD) versus microbiome from control SPF (GF+SPF) mice at ZT2 and (F) GF mice mono-colonized with mouse/rat segmented filamentous bacteria (GF+M.SFB and GF+R.SFB, respectively) at ZT2.
(H–J) Frequency of SI CD4$^+$CD8a$^-$TCR-$\alpha\beta^+$TCR-$\gamma\delta^-$ Foxp3$^-$IL-4$^-$IL-10$^+$ IELs of (H) Villin-cre I-Ab fl/fl mice versus I-Ab fl/fl littermates, (I) Villin-cre CDC42 fl/fl versus CDC42 fl/fl, and (J) SAA KO versus WT at ZT8 and ZT0. All data represent at least two independent experiments.
Means ± SD are plotted. *p < 0.05, **p < 0.01, ***p < 0.001, ****p < 0.0001 by Mann-Whitney U test. See also Figures S5 and S6.

Please cite this article in press as: Tuganbaev et al., Diet Diurnally Regulates Small Intestinal Microbiome-Epithelial-Immune Homeostasis and Enteritis, Cell (2020), https://doi.org/10.1016/j.cell.2020.08.027

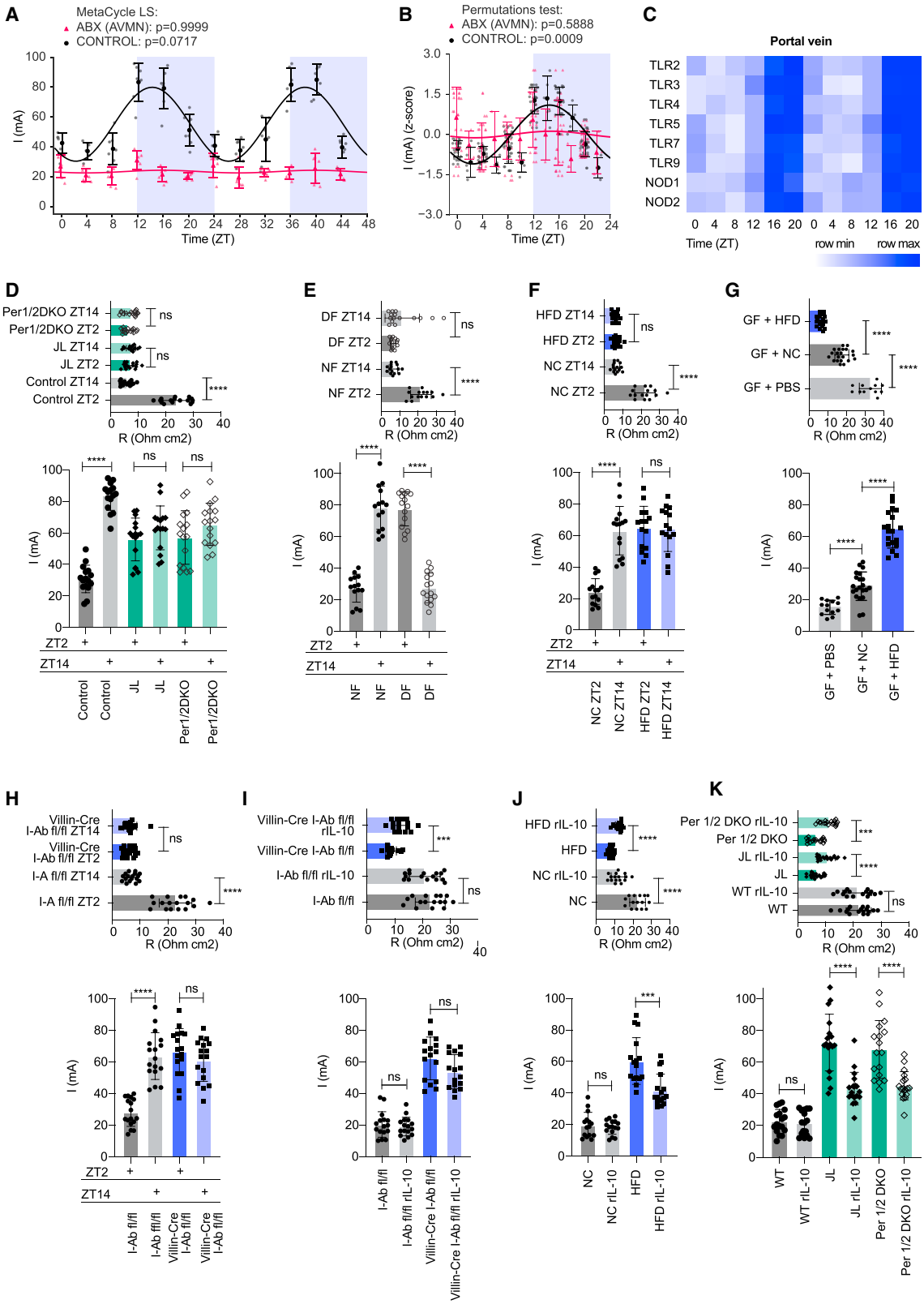

(legend on next page)

Please cite this article in press as: Tuganbaev et al., Diet Diurnally Regulates Small Intestinal Microbiome-Epithelial-Immune Homeostasis and Enteritis, Cell (2020), https://doi.org/10.1016/j.cell.2020.08.027

recombinant IL-10 (rIL-10) to Villin-Cre I-Ab$^{fl/fl}$ mice (Figure 6I, pooled results, three independent repeats; Figures S8A and S8B), to HFD fed mice (Figure 6J, pooled results, three independent repeats; Figure S8C), or to Per1/2 DKO mice and jet-lagged mice (Figure 6K, pooled results, three independent repeats; Figure S8D) significantly improved gut barrier dysfunction in these settings. CDC42-mediated endocytosis potentially participated in regulation of SI barrier function, as PRR ligand concentrations at ZT2 and ZT10 in peripheral blood (Figure S8E) and liver (Figure S8F) of Villin-Cre CDC42$^{fl/fl}$ mice were increased as compared to CDC42$^{fl/fl}$ littermate controls. Collectively, the aforementioned studies suggest that the dietary-microbiome-SIEC MHC class II-IL-10 axis contributes to control of a diurnally variating SI barrier function.

Impairment in the Dietary-Microbiome-SIEC MHC Class II Barrier Integrity Axis Exacerbates Crohn-like Enteritis

Finally, we explored potential physiological roles of SIEC MHC class II in modulating a murine model of SI CD. To this aim, we utilized a CD4$^+$ T cell transfer-mediated model of IBD that manifests in SI as Crohn-like enteritis by transferring 1.5*10^6 naive T cells (CD4$^+$CD25$^-$CD44^{Low}CD62L^{hi}CD45RB^{hi}) into 8-week-old male Villin-Cre-I-Ab$^{fl/fl}$-Rag1$^{-/-}$ mice or into I-Ab$^{fl/fl}$ Rag1$^{-/-}$ littermate controls (Figure S8G). Four weeks later, mice were sacrificed and SI histology, barrier function, and MHC class II expression were assessed. Importantly, recipient Villin-Cre-I-Ab$^{fl/fl}$-Rag1$^{-/-}$ mice featured an enhanced weight loss compared to recipient littermate I-Ab$^{fl/fl}$-Rag1$^{-/-}$ mice (Figure 7A, pooled results, two independent repeats), driven by worsened inflammation by histological score, characterized by transmural inflammation, dense infiltrates involving neutrophils, and crypt abscesses (Figure 7B, exemplary histology panels, Figure 7C, histological quantification, pooled results, two independent repeats). These histopathological changes were coupled with increased SI permeability (Figure 7D, pooled results, two independent repeats) and reduced frequency of IL-10$^+$CD4$^+$ IELs (Figure 7E, pooled results, two independent repeats), collectively suggesting that SIEC MHC class II plays a protective role in this SI inflammatory setting.

To further delineate the role of SIEC MHC class II diurnal regulation, we next implemented the chronic jet-lag protocol in the context of T cell transfer-mediated enteritis in I-Ab$^{fl/fl}$ -Rag1$^{-/-}$ mice. Indeed, jet lag resulted in an accelerated weight loss (Figure 7F), reduced SIEC MHC class II expression (Figure 7G), increased SI ion permeability (Figure 7H), and reduced frequency of IL-10$^+$CD4$^+$ IELs (Figure 7I) in recipient mice, suggesting that temporal regulation of SIEC MHC class II is necessary in regulating SI immune response and barrier function. Supplementation of rIL-10 to Villin-Cre I-Ab$^{fl/fl}$-Rag1$^{-/-}$ mice upon induction of adoptive T cell transfer-mediated enteritis ameliorated weight loss (Figure 7J), decreased SI ion permeability (Figure 7L), but had no effect on SIEC MHC class II expression (Figure 7K) or the frequency of IL-10$^+$CD4$^+$ IELs (Figure 7M), supporting the notion that IL-10 activity is downstream of SIEC MHC class II. Collectively, these results suggest that the aforementioned dietary-microbiome-host mucosal immune axis regulates SI immune homeostasis, while its disruption contributes to SI auto-inflammation.

DISCUSSION

In this study, we uncover how feeding composition and rhythmicity modulate the SI barrier function, by shaping the SI microbiome, and regulating SIEC crosstalk with IEL across a 24-h cycle. We highlight diurnally shifting MHC class II expression (Christ and Blumberg, 1997) in SIECs to be a signaling conduit, interconnecting extrinsic microbial and dietary cues with diurnal activity of CD4$^+$CD8a$^-$TCR-$\alpha\beta^+$TCR-$\gamma\delta^-$IL-10$^+$IL-4$^-$Foxp3$^-$ IELs, which, in turn, diurnally secrete IL-10 (Das et al., 2003; Sujino et al., 2016), ultimately driving a higher SI permeability and tissue tolerance during the active phase and a lower permeability and tissue tolerance during the resting phase (summary schematic available at https://data.mendeley.com/datasets/wp2wt38pdg/draft?a+1bb5fe57-453f-4b05-b558-43207bb705b8a**)**. Disruption of this diurnally regulated diet-microbiome-SIEC MHC class II-IL-10 axis by host circadian clock disruption, dietary alterations, or epithelial-specific MHC class II depletion leads to commensal-dependent impairment of the SI barrier function and extensive microbial product influx, contributing to exacerbated Crohn-like enteritis. This axis, to be further explored in future studies, may present a mechanistic explanation for the observed reduction of IELs noted in patients with Celiac disease (Carton et al., 2004) and supports the IEL tolerogenic role observed in experimental models of IBD (McDonald et al., 2018).

Additionally, our study identifies the SI microbiome as a central module responding to nutritional inputs, such as feeding composition and rhythmicity, by altering its composition, to enable relay of environmental signals to host SIECs across a 24-h cycle. Through this activity, one may speculate that the

Figure 6. Dietary Composition and Rhythm Regulate SI Permeability through SI Microbiome

(A and B) Distal jejunum trans-epithelial ion permeability of mice treated with AVMN antibiotics cocktail versus control mice every 4 h across 48 h (A) and in an average of two consecutive 24-h cycles (B). The line represents the sine fit curve, and p values were calculated by LS test for 48 h (A) or by PT for 24 h (B).

(C) Heatmap of pattern recognition receptors (PRR) stimulation by portal vein serum collected every 4 h across two consecutive 24-h cycles. n = 4–6 mice per time point.

(D–F) Distal jejunum trans-epithelial ion permeability and resistance of (D) Per1/2 DKO mice versus jet-lagged mice (JL) versus controls at ZT2 versus ZT14, (E) day fed versus night fed, and (F) HFD fed versus NC fed mice.

(G) Distal jejunum trans-epithelial ion permeability and resistance of germ-free (GF) mice reconstituted with luminal SI microbiome of HFD-fed mice (GF+HFD) versus microbiome from control SPF mice (GF+NC) at ZT2.

(H) Distal jejunum trans-epithelial ion permeability and resistance of Villin-cre I-Ab fl/fl mice versus I-Ab fl/fl littermates at ZT2 versus ZT14.

(I–K) Distal jejunum trans-epithelial ion permeability and resistance of (I) Villin-cre I-Ab fl/fl mice versus I-Ab fl/fl littermates, (J) HFD fed versus NC fed mice, and (K) Per1/2 DKO mice versus jet-lagged mice (JL) versus controls at ZT2. All groups were systemically administered rIL-10 versus PBS. All data represent at least two independent experiments.

Means ± SD are plotted. *p < 0.05, **p < 0.01, ***p < 0.001, ****p < 0.0001 by Mann-Whitney U test. See also Figures S6, S7, and S8.

Please cite this article in press as: Tuganbaev et al., Diet Diurnally Regulates Small Intestinal Microbiome-Epithelial-Immune Homeostasis and Enteritis, Cell (2020), https://doi.org/10.1016/j.cell.2020.08.027

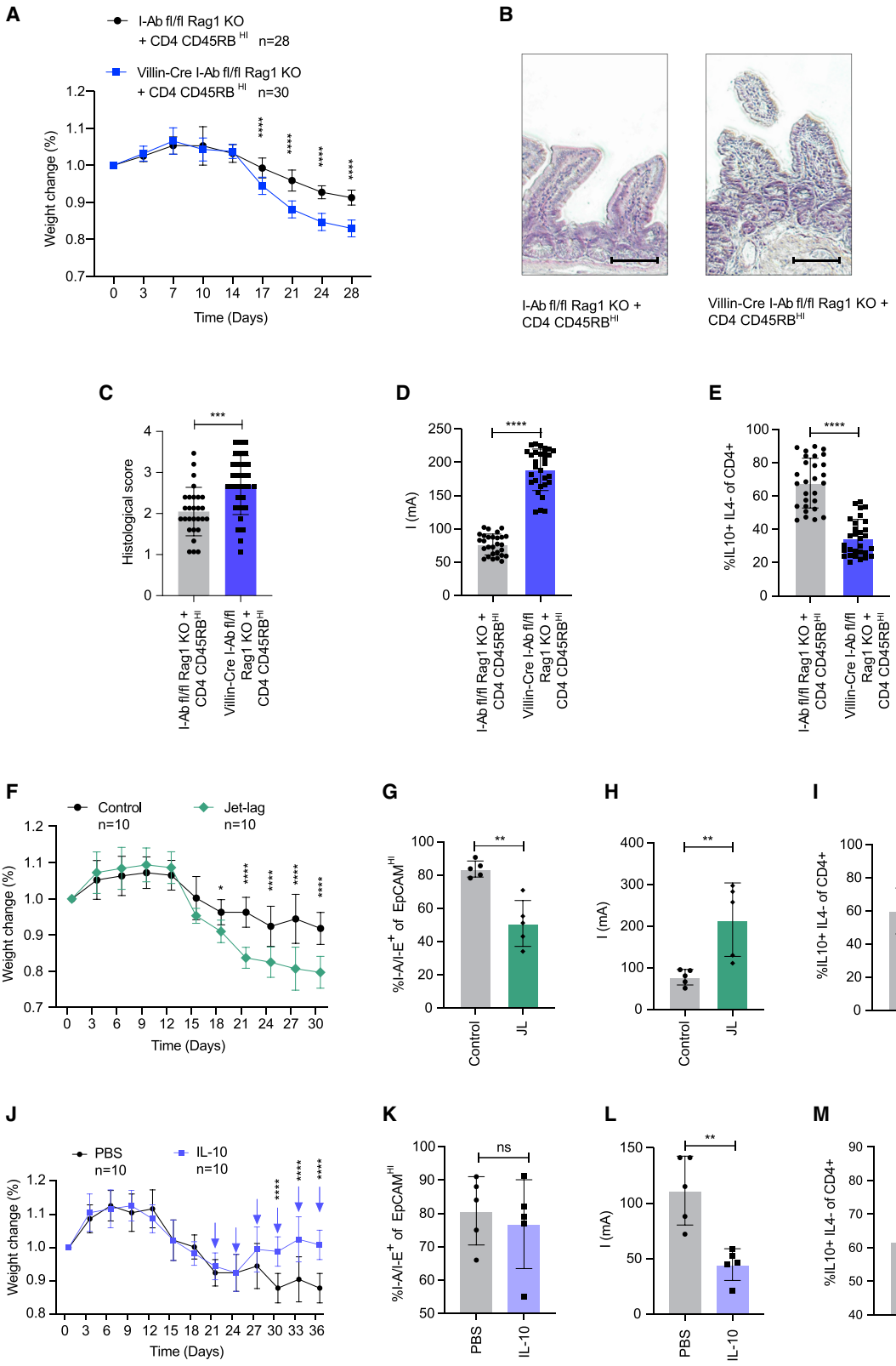

(legend on next page)

dynamically shifting SI microbiome enables the host to anticipate incoming nutrient availability, accordingly adapt its SI absorptive machinery, and synchronize the tolerogenic activity of intra-epithelial first line immune responders to an anticipated increase in antigenic burden. We envision a diurnal SIEC reactivity to nutritional and microbiome signals as potentially constituting an important organizational principle of host-microbiome meta-organismal cooperation, jointly orchestrating the SI barrier function and associated mucosal immunity. Disruption of any of the components of this metaorganismal SI host-microbiome axis can deleteriously impact SI barrier integrity. Such disruption, in turn, may contribute to an exacerbated SI inflammation culminating in Crohn-like enteritis in susceptible hosts.

Future animal and human studies may delineate the relevance of the principles highlighted by our study to increased risk of CD exacerbation upon disruption of the sleep-wake cycle (Liu et al., 2017; Palmieri et al., 2015; Sobolewska-Włodarczyk et al., 2016; Swanson and Burgess, 2017), and the observed efficacy of nutritional interventions in some CD patient subsets, including elemental enteric nutrition (Ashton et al., 2019), specific carbohydrates (Brandes et al., 1982; Brandes and Lorenz-Meyer, 1981; Cohen et al., 2014; Järnerot et al., 1983; Ritchie et al., 1987), protein and poly-unsaturated fatty acids (Feagan et al., 2008; Stange et al., 1990), and fiber (Ananthakrishnan et al., 2014; Ananthakrishnan et al., 2013; Brotherton et al., 2014). Such mechanistic insights may help delineate new person-specific dietary, microbiome, and SIEC-targeted interventions, aimed at utilizing checkpoints along this axis toward restoring barrier function and tissue tolerance in SI auto-inflammatory disorders.

Limitations of Study

Our study focused on exploring the effects of nutrition and the microbiome on SIEC interactions with IEL, which may impact downstream barrier function and inflammatory capacity in both direct and indirect manners. Other IEC-immune interactions may indirectly affect downstream barrier function and inflammation and merit further studies. Additionally, a residual 40% SIEC MHC class II expression noted upon exposure to HFD (Figure 3B) may point to the presence of SIEC subsets that feature a stable, rather than diurnally shifting MHC class II expression pattern and merit further studies. Likewise, the intricate details of molecular machinery regulating SIEC MHC class II expression and its interplay with microbial adhesion events constitute promising avenues of future research.

STAR★METHODS

Detailed methods are provided in the online version of this paper and include the following:

- KEY RESOURCES TABLE
- RESOURCE AVAILABILITY
  - Lead Contact
  - Materials Availability
  - Data and Code Availability
- EXPERIMENTAL MODEL AND SUBJECT DETAILS
  - Mice
- METHOD DETAILS
  - Taxonomic Microbiome Analysis
  - Library preparation for mcSCRB-seq
  - mcSCRB-seq analysis
  - Single-molecule fluorescence *in situ* hybridization (smFISH)
  - Image analysis
  - Flow Cytometry Analysis (FACS)
  - Ussing chamber
  - Measuring Colonic Epithelial Barrier Permeability by FITC-dextran
  - Quantification of microbial products at systemic sites
  - Purification of intestinal epithelial cells for RNA isolation
  - Treatment with chemical inhibitors in externalized intestinal loops
  - Bacterial isolation
  - Fecal Microbiome Transplantation (FMT)
  - Adoptive T cell transfer mediated enteritis
  - Treatment with rIL–10
  - Histology
  - Data integrity check
- QUANTIFICATION AND STATISTICAL ANALYSIS

SUPPLEMENTAL INFORMATION

Supplemental Information can be found online at https://doi.org/10.1016/j.cell.2020.08.027.

Figure 7. Disruption of Diet-Microbiome-MHC Class II-IL-10 Axis Exacerbates Crohn-like Enteritis

(A–C) Weight change (A), representative histological samples, scale bar 100 μm (B) and histological score (C) of Villin-cre I-Ab fl/fl Rag1$^{-/-}$ versus I-Ab fl/fl Rag1$^{-/-}$ littermate mice systemically administered CD4^{+}CD45RB^{hi} lymphocytes.

(D and E) Distal jejunum trans-epithelial ion permeability (D) and frequency of IL-10^{+} cells from SI CD4^{+}CD8a^{-}TCR-αβ^{+}TCR-γδ^{-} intraepithelial lymphocytes (E) of Villin-cre I-Ab fl/fl Rag1$^{-/-}$ versus I-Ab fl/fl Rag1$^{-/-}$ littermate mice systemically administered with CD4^{+}CD45RB^{hi} lymphocytes.

(F) Weight change of jet lag versus control mice systemically administered CD4^{+}CD45RB^{hi} lymphocytes.

(G–I) Frequency of MHC class II^{+}CD45^{-}EpCAM^{hi} SIECs (G), distal jejunum trans-epithelial ion permeability (H), and frequency of IL-10^{+} cells from SI CD4^{+}CD8a^{-}TCR-αβ^{+}TCR-γδ^{-} intraepithelial lymphocytes (I) of jet-lagged mice versus littermate mice systemically administered with CD4^{+}CD45RB^{hi} lymphocytes.

(J) Weight change of Villin-cre I-Ab fl/fl Rag1$^{-/-}$ versus I-Ab fl/fl Rag1$^{-/-}$ littermate mice treated with of rIL-10 systemically every 3 days for 2 weeks. Arrows represent IL-10 treatment.

(K–M) Distal jejunum trans-epithelial ion permeability (K), frequency of MHC class II^{+}CD45^{-}EpCAM^{hi} SIECs (L), and frequency of IL-10 derived from SI CD4^{+}CD8α^{-}TCR-αβ^{+}TCR-γδ^{-} intraepithelial lymphocytes (M) of Villin-cre I-Ab fl/fl Rag1$^{-/-}$ versus I-Ab fl/fl Rag1$^{-/-}$ littermate mice treated with rIL-10 systemically. All data represent at least two independent experiments.

Means ± SD are plotted. *p < 0.05, **p < 0.01, ***p < 0.001, ****p < 0.0001 by Mann-Whitney U test unless stated otherwise. Two-way ANOVA test was used for Figures 7A, 7F, and 7J. See also Figure S8.

ACKNOWLEDGMENTS

We thank the members of the E.E. lab for discussions and apologize to authors whose work was not included due to space constraints. We thank Idit Shachar and Yifat Merbl, Weizmann Institute of Science, for suggestions. We thank Carmit Bar-Nathan for assistance with animal work; Steffen Jung, Weizmann Institute of Science, for providing MHC class II$^{fl/fl}$ mice; and Jeremiah Faith, Mount Sinai School of Medicine, for generously providing GF Rag$^{-/-}$ mice. We thank Maria Eizner of Eizner Design for graphical design support. T.L. is funded as postdoctoral fellow by the German Research Foundation (DFG, 420943353). S.P.N. is funded by an EMBO Long term Fellowship ATF 767-2017. E.E. is supported by Y. and R. Ungar, the Abisch Frenkel Foundation for the Promotion of Life Sciences, the Gurwin Family Fund for Scientific Research, the Leona M. and Harry B. Helmsley Charitable Trust, the Crown Endowment Fund for Immunological Research, the Else Kroener Fresenius Foundation, the estate of J. Gitlitz, the estate of L. Hershkovich, the Benoziyo Endowment Fund for the Advancement of Science, the Adelis Foundation, J.L. and V. Schwartz, A. and G. Markovitz, A. and C. Adelson, the French National Center for Scientific Research (CNRS), D.L. Schwarz, The V.R. Schwartz Research Fellow Chair, L. Steinberg, J.N. Halpern, A. Edelheit, and by grants funded by the European Research Council, a Marie Curie Integration grant, the German-Israeli Foundation for Scientific Research and Development, the Israel Science Foundation, the Helmholtz Foundation, and the European Foundation for the Study of Diabetes. E.E. is a senior fellow, Canadian Institute of Advanced Research (CIFAR) and an international scholar, Howard Hughes Medical Institute (HHMI).

AUTHOR CONTRIBUTIONS

T.T., H.S., and E.E. conceived the study; designed, performed, and interpreted the experiments; and wrote the manuscript. U.M. headed and performed all computational analyses and pipeline development and equally contributed to the study. S.P.N., H.S., and K.R. independently reproduced key experiments of the study. T.L., L.K.A., Y.C., and H.M. performed bioinformatics and statistical analysis. S.B., A.L., E.Y.P., S.F., C.K., C.M., Y.K., M.D.-B., C.A.T., T.Y., X.Z., and H.S. helped with experiments. H.M. and E.M. performed smFISH. P.A.K., A.H., N.G., S.I., and K.H. provided essential tools and insights.

DECLARATION OF INTERESTS

E.E. is a consultant to DayTwo and BiomX. None of the topics related to this work involve these or other commercial entities. None of the other authors have any financial or non-financial competing interest.

Received: March 14, 2019
Revised: April 27, 2020
Accepted: August 14, 2020
Published: September 3, 2020

REFERENCES

Ananthakrishnan, A.N., Khalili, H., Konijeti, G.G., Higuchi, L.M., de Silva, P., Korzenik, J.R., Fuchs, C.S., Willett, W.C., Richter, J.M., and Chan, A.T. (2013). A prospective study of long-term intake of dietary fiber and risk of Crohn's disease and ulcerative colitis. Gastroenterology *145*, 970–977.

Ananthakrishnan, A.N., Khalili, H., Konijeti, G.G., Higuchi, L.M., de Silva, P., Fuchs, C.S., Willett, W.C., Richter, J.M., and Chan, A.T. (2014). Long-term intake of dietary fat and risk of ulcerative colitis and Crohn's disease. Gut *63*, 776–784.

Ashton, J.J., Gavin, J., and Beattie, R.M. (2019). Exclusive enteral nutrition in Crohn's disease: Evidence and practicalities. Clin. Nutr. *38*, 80–89.

Atarashi, K., Tanoue, T., Ando, M., Kamada, N., Nagano, Y., Narushima, S., Suda, W., Imaoka, A., Setoyama, H., Nagamori, T., et al. (2015). Th17 Cell Induction by Adhesion of Microbes to Intestinal Epithelial Cells. Cell *163*, 367–380.

Bae, K., Jin, X., Maywood, E.S., Hastings, M.H., Reppert, S.M., and Weaver, D.R. (2001). Differential functions of mPer1, mPer2, and mPer3 in the SCN circadian clock. Neuron *30*, 525–536.

Bagnoli, J.W., Ziegenhain, C., Janjic, A., Wange, L.E., Vieth, B., Parekh, S., Geuder, J., Hellmann, I., and Enard, W. (2018). Sensitive and powerful single-cell RNA sequencing using mcSCRB-seq. Nat. Commun. *9*, 2937.

Biton, M., Haber, A.L., Rogel, N., Burgin, G., Beyaz, S., Schnell, A., Ashenberg, O., Su, C.W., Smillie, C., Shekhar, K., et al. (2018). T Helper Cell Cytokines Modulate Intestinal Stem Cell Renewal and Differentiation. Cell *175*, 1307–1320.

Bolyen, E., Rideout, J.R., Dillon, M.R., Bokulich, N.A., Abnet, C.C., Al-Ghalith, G.A., Alexander, H., Alm, E.J., Arumugam, M., Asnicar, F., et al. (2019). Reproducible, interactive, scalable and extensible microbiome data science using QIIME 2. Nat. Biotechnol. *37*, 852–857.

Brandes, J.W., and Lorenz-Meyer, H. (1981). [Sugar free diet: a new perspective in the treatment of Crohn disease? Randomized, control study]. Z. Gastroenterol. *19*, 1–12.

Brandes, J.W., Körst, H.A., and Littman, K.P. (1982). [Sugar-free diet as long-term or interval treatment in the remission phase of Crohn disease–a prospective study]. Leber Magen Darm *12*, 225–228.

Brotherton, C.S., Taylor, A.G., Bourguignon, C., and Anderson, J.G. (2014). A high-fiber diet may improve bowel function and health-related quality of life in patients with Crohn disease. Gastroenterol. Nurs. *37*, 206–216.

Büning, J., Schmitz, M., Repenning, B., Ludwig, D., Schmidt, M.A., Strobel, S., and Zimmer, K.P. (2005). Interferon-gamma mediates antigen trafficking to MHC class II-positive late endosomes of enterocytes. Eur. J. Immunol. *35*, 831–842.

Callahan, B.J., McMurdie, P.J., Rosen, M.J., Han, A.W., Johnson, A.J., and Holmes, S.P. (2016). DADA2: High-resolution sample inference from Illumina amplicon data. Nat. Methods *13*, 581–583.

Canfora, E.E., Jocken, J.W., and Blaak, E.E. (2015). Short-chain fatty acids in control of body weight and insulin sensitivity. Nat. Rev. Endocrinol. *11*, 577–591.

Cani, P.D., Possemiers, S., Van de Wiele, T., Guiot, Y., Everard, A., Rottier, O., Geurts, L., Naslain, D., Neyrinck, A., Lambert, D.M., et al. (2009). Changes in gut microbiota control inflammation in obese mice through a mechanism involving GLP-2-driven improvement of gut permeability. Gut *58*, 1091–1103.

Carton, J., Byrne, B., Madrigal-Estebas, L., O'Donoghue, D.P., and O'Farrelly, C. (2004). CD4+CD8+ human small intestinal T cells are decreased in coeliac patients, with CD8 expression downregulated on intra-epithelial T cells in the active disease. Eur. J. Gastroenterol. Hepatol. *16*, 961–968.

Chaix, A., Zarrinpar, A., Miu, P., and Panda, S. (2014). Time-restricted feeding is a preventative and therapeutic intervention against diverse nutritional challenges. Cell Metab. *20*, 991–1005.

Christ, A.D., and Blumberg, R.S. (1997). The intestinal epithelial cell: immunological aspects. Springer Semin. Immunopathol. *18*, 449–461.

Cohen, S.A., Gold, B.D., Oliva, S., Lewis, J., Stallworth, A., Koch, B., Eshee, L., and Mason, D. (2014). Clinical and mucosal improvement with specific carbohydrate diet in pediatric Crohn disease. J. Pediatr. Gastroenterol. Nutr. *59*, 516–521.

Cummins, A.G., Penttila, I.A., Labrooy, J.T., Robb, T.A., and Davidson, G.P. (1991). Recovery of the small intestine in coeliac disease on a gluten-free diet: changes in intestinal permeability, small bowel morphology and T-cell activity. J. Gastroenterol. Hepatol. *6*, 53–57.

Das, G., Augustine, M.M., Das, J., Bottomly, K., Ray, P., and Ray, A. (2003). An important regulatory role for CD4+CD8 alpha alpha T cells in the intestinal epithelial layer in the prevention of inflammatory bowel disease. Proc. Natl. Acad. Sci. USA *100*, 5324–5329.

Eri, R., McGuckin, M.A., and Wadley, R. (2012). T cell transfer model of colitis: a great tool to assess the contribution of T cells in chronic intestinal inflammation. Methods Mol. Biol. *844*, 261–275.

Feagan, B.G., Sandborn, W.J., Mittmann, U., Bar-Meir, S., D'Haens, G., Bradette, M., Cohen, A., Dallaire, C., Ponich, T.P., McDonald, J.W., et al. (2008).

Omega-3 free fatty acids for the maintenance of remission in Crohn disease: the EPIC Randomized Controlled Trials. JAMA *299*, 1690–1697.

Flannigan, K.L., Agbor, T.A., Blackler, R.W., Kim, J.J., Khan, W.I., Verdu, E.F., Ferraz, J.G., and Wallace, J.L. (2014). Impaired hydrogen sulfide synthesis and IL-10 signaling underlie hyperhomocysteinemia-associated exacerbation of colitis. Proc. Natl. Acad. Sci. USA *111*, 13559–13564.

Gil-Lozano, M., Wu, W.K., Martchenko, A., and Brubaker, P.L. (2016). High-Fat Diet and Palmitate Alter the Rhythmic Secretion of Glucagon-Like Peptide-1 by the Rodent L-cell. Endocrinology *157*, 586–599.

Glynn, E.F., Chen, J., and Mushegian, A.R. (2006). Detecting periodic patterns in unevenly spaced gene expression time series using Lomb-Scargle periodograms. Bioinformatics *22*, 310–316.

Gonnella, P.A., and Wilmore, D.W. (1993). Co-localization of class II antigen and exogenous antigen in the rat enterocyte. J. Cell Sci. *106*, 937–940.

Goo, R.H., Moore, J.G., Greenberg, E., and Alazraki, N.P. (1987). Circadian variation in gastric emptying of meals in humans. Gastroenterology *93*, 515–518.

Hashimoto, K., Joshi, S.K., and Koni, P.A. (2002). A conditional null allele of the major histocompatibility IA-beta chain gene. Genesis *32*, 152–153.

Hershberg, R.M., Framson, P.E., Cho, D.H., Lee, L.Y., Kovats, S., Beitz, J., Blum, J.S., and Nepom, G.T. (1997). Intestinal epithelial cells use two distinct pathways for HLA class II antigen processing. J. Clin. Invest. *100*, 204–215.

Hoogerwerf, W.A., Shahinian, V.B., Cornélissen, G., Halberg, F., Bostwick, J., Timm, J., Bartell, P.A., and Cassone, V.M. (2010). Rhythmic changes in colonic motility are regulated by period genes. Am. J. Physiol. Gastrointest. Liver Physiol. *298*, G143–G150.

Hughes, M.E., Hogenesch, J.B., and Kornacker, K. (2010). JTK_CYCLE: an efficient nonparametric algorithm for detecting rhythmic components in genome-scale data sets. J. Biol. Rhythms *25*, 372–380.

Järnerot, G., Järnmark, I., and Nilsson, K. (1983). Consumption of refined sugar by patients with Crohn's disease, ulcerative colitis, or irritable bowel syndrome. Scand. J. Gastroenterol. *18*, 999–1002.

Koyama, M., Mukhopadhyay, P., Schuster, I.S., Henden, A.S., Hulsdunker, J., Varelias, A., Vetizou, M., Kuns, R.D., Robb, R.J., Zhang, P., et al. (2019). MHC Class II Antigen Presentation by the Intestinal Epithelium Initiates Graft-versus-Host Disease and Is Influenced by the Microbiota. Immunity Immunity *51*, 885–898.

Kumar, D., Wingate, D., and Ruckebusch, Y. (1986). Circadian variation in the propagation velocity of the migrating motor complex. Gastroenterology *91*, 926–930.

Kunisawa, J., Gohda, M., Hashimoto, E., Ishikawa, I., Higuchi, M., Suzuki, Y., Goto, Y., Panea, C., Ivanov, I.I., Sumiya, R., et al. (2013). Microbe-dependent CD11b+ IgA+ plasma cells mediate robust early-phase intestinal IgA responses in mice. Nat. Commun. *4*, 1772.

Ladinsky, M.S., Araujo, L.P., Zhang, X., Veltri, J., Galan-Diez, M., Soualhi, S., Lee, C., Irie, K., Pinker, E.Y., Narushima, S., et al. (2019). Endocytosis of commensal antigens by intestinal epithelial cells regulates mucosal T cell homeostasis. Science *363*, eaat4042.

Lau, J.T., Whelan, F.J., Herath, I., Lee, C.H., Collins, S.M., Bercik, P., and Surette, M.G. (2016). Capturing the diversity of the human gut microbiota through culture-enriched molecular profiling. Genome Med. *8*, 72.

Lázár-Molnár, E., and Snyder, M. (2018). The Role of Human Leukocyte Antigen in Celiac Disease Diagnostics. Clin. Lab. Med. *38*, 655–668.

Lemmer, B., and Nold, G. (1991). Circadian changes in estimated hepatic blood flow in healthy subjects. Br. J. Clin. Pharmacol. *32*, 627–629.

Levy, M., Thaiss, C.A., Zeevi, D., Dohnalová, L., Zilberman-Schapira, G., Mahdi, J.A., David, E., Savidor, A., Korem, T., Herzig, Y., et al. (2015). Microbiota-Modulated Metabolites Shape the Intestinal Microenvironment by Regulating NLRP6 Inflammasome Signaling. Cell *163*, 1428–1443.

Liu, X., Yu, R., Zhu, L., Hou, X., and Zou, K. (2017). Bidirectional Regulation of Circadian Disturbance and Inflammation in Inflammatory Bowel Disease. Inflamm. Bowel Dis. *23*, 1741–1751.

Lomb, N.R. (1976). Least-squares frequency analysis of unequally spaced data. Astrophys. Space Sci. *39*, 447–462.

McDonald, B.D., Jabri, B., and Bendelac, A. (2018). Diverse developmental pathways of intestinal intraepithelial lymphocytes. Nat. Rev. Immunol. *18*, 514–525.

Moor, A.E., Golan, M., Massasa, E.E., Lemze, D., Weizman, T., Shenhav, R., Baydatch, S., Mizrahi, O., Winkler, R., Golani, O., et al. (2017). Global mRNA polarization regulates translation efficiency in the intestinal epithelium. Science *357*, 1299–1303.

Moor, A.E., Harnik, Y., Ben-Moshe, S., Massasa, E.E., Rozenberg, M., Eilam, R., Bahar Halpern, K., and Itzkovitz, S. (2018). Spatial Reconstruction of Single Enterocytes Uncovers Broad Zonation along the Intestinal Villus Axis. Cell *175*, 1156–1167.

Palmieri, O., Mazzoccoli, G., Bossa, F., Maglietta, R., Palumbo, O., Ancona, N., Corritore, G., Latiano, T., Martino, G., Rubino, R., et al. (2015). Systematic analysis of circadian genes using genome-wide cDNA microarrays in the inflammatory bowel disease transcriptome. Chronobiol. Int. *32*, 903–916.

Pan, X., and Hussain, M.M. (2009). Clock is important for food and circadian regulation of macronutrient absorption in mice. J. Lipid Res. *50*, 1800–1813.

Powrie, F., Leach, M.W., Mauze, S., Menon, S., Caddle, L.B., and Coffman, R.L. (1994). Inhibition of Th1 responses prevents inflammatory bowel disease in scid mice reconstituted with CD45RBhi CD4+ T cells. Immunity *1*, 553–562.

Ridaura, V.K., Faith, J.J., Rey, F.E., Cheng, J., Duncan, A.E., Kau, A.L., Griffin, N.W., Lombard, V., Henrissat, B., Bain, J.R., et al. (2013). Gut microbiota from twins discordant for obesity modulate metabolism in mice. Science *341*, 1241214.

Ritchie, J.K., Wadsworth, J., Lennard-Jones, J.E., and Rogers, E. (1987). Controlled multicentre therapeutic trial of an unrefined carbohydrate, fibre rich diet in Crohn's disease. Br. Med. J. (Clin. Res. Ed.) *295*, 517–520.

Sakamori, R., Yu, S., Zhang, X., Hoffman, A., Sun, J., Das, S., Vedula, P., Li, G., Fu, J., Walker, F., et al. (2014). CDC42 inhibition suppresses progression of incipient intestinal tumors. Cancer Res. *74*, 5480–5492.

Schneider, C.A., Rasband, W.S., and Eliceiri, K.W. (2012). NIH Image to ImageJ: 25 years of image analysis. Nat. Methods *9*, 671–675.

Senju, M., Wu, K.C., Mahida, Y.R., and Jewell, D.P. (1991). Coexpression of CD4 and CD8 on peripheral blood T cells and lamina propria T cells in inflammatory bowel disease by two colour immunofluorescence and flow cytometric analysis. Gut *32*, 918–922.

Sobolewska-Włodarczyk, A., Włodarczyk, M., Szemraj, J., Stec-Michalska, K., Fichna, J., and Wiśniewska-Jarosińska, M. (2016). Circadian rhythm abnormalities: Association with the course of inflammatory bowel disease. Pharmacol. Rep. *68*, 847–851.

Stange, E.F., Schmid, U., Fleig, W.E., and Ditschuneit, H. (1990). [Exclusion diet in Crohn disease: a controlled, randomized study]. Z. Gastroenterol. *28*, 561–564.

Suez, J., Zmora, N., Zilberman-Schapira, G., Mor, U., Dori-Bachash, M., Bashiardes, S., Zur, M., Regev-Lehavi, D., Ben-Zeev Brik, R., Federici, S., et al. (2018). Post-Antibiotic Gut Mucosal Microbiome Reconstitution Is Impaired by Probiotics and Improved by Autologous FMT. Cell *174*, 1406–1423.

Sujino, T., London, M., Hoytema van Konijnenburg, D.P., Rendon, T., Buch, T., Silva, H.M., Lafaille, J.J., Reis, B.S., and Mucida, D. (2016). Tissue adaptation of regulatory and intraepithelial $CD4^+$ T cells controls gut inflammation. Science *352*, 1581–1586.

Swanson, G.R., and Burgess, H.J. (2017). Sleep and Circadian Hygiene and Inflammatory Bowel Disease. Gastroenterol. Clin. North Am. *46*, 881–893.

Thaiss, C.A., Zeevi, D., Levy, M., Zilberman-Schapira, G., Suez, J., Tengeler, A.C., Abramson, L., Katz, M.N., Korem, T., Zmora, N., et al. (2014). Transkingdom control of microbiota diurnal oscillations promotes metabolic homeostasis. Cell *159*, 514–529.

Thaiss, C.A., Zeevi, D., Levy, M., Segal, E., and Elinav, E. (2015). A day in the life of the meta-organism: diurnal rhythms of the intestinal microbiome and its host. Gut Microbes *6*, 137–142.

Thaiss, C.A., Levy, M., Korem, T., Dohnalova, L., Shapiro, H., Jaitin, D.A., David, E., Winter, D.R., Gury-BenAri, M., Tatirovsky, E., et al. (2016). Microbiota Diurnal Rhythmicity Programs Host Transcriptome Oscillations. Cell *167*, 1495–1510.

Thaiss, C.A., Levy, M., Grosheva, I., Zheng, D., Soffer, E., Blacher, E., Braverman, S., Tengeler, A.C., Barak, O., Elazar, M., et al. (2018). Hyperglycemia drives intestinal barrier dysfunction and risk for enteric infection. Science *359*, 1376–1383.

Thomas, C., Gioiello, A., Noriega, L., Strehle, A., Oury, J., Rizzo, G., Macchiarulo, A., Yamamoto, H., Mataki, C., Pruzanski, M., et al. (2009). TGR5-mediated bile acid sensing controls glucose homeostasis. Cell Metab. *10*, 167–177.

Tognini, P., Thaiss, C.A., Elinav, E., and Sassone-Corsi, P. (2017). Circadian Coordination of Antimicrobial Responses. Cell Host Microbe *22*, 185–192.

Turnbaugh, P.J., Ley, R.E., Mahowald, M.A., Magrini, V., Mardis, E.R., and Gordon, J.I. (2006). An obesity-associated gut microbiome with increased capacity for energy harvest. Nature *444*, 1027–1031.

Vezys, V., Olson, S., and Lefrançois, L. (2000). Expression of intestine-specific antigen reveals novel pathways of CD8 T cell tolerance induction. Immunity *12*, 505–514.

Vrieze, A., Van Nood, E., Holleman, F., Salojarvi, J., Kootte, R.S., Bartelsman, J.F., Dallinga-Thie, G.M., Ackermans, M.T., Serlie, M.J., Oozeer, R., et al. (2012). Transfer of intestinal microbiota from lean donors increases insulin sensitivity in individuals with metabolic syndrome. Gastroenterology *143*, 913–916.

Westendorf, A.M., Fleissner, D., Groebe, L., Jung, S., Gruber, A.D., Hansen, W., and Buer, J. (2009). CD4+Foxp3+ regulatory T cell expansion induced by antigen-driven interaction with intestinal epithelial cells independent of local dendritic cells. Gut *58*, 211–219.

Wu, G., Anafi, R.C., Hughes, M.E., Kornacker, K., and Hogenesch, J.B. (2016). MetaCycle: an integrated R package to evaluate periodicity in large scale data. Bioinformatics *32*, 3351–3353.

Zarrinpar, A., Chaix, A., Yooseph, S., and Panda, S. (2014). Diet and feeding pattern affect the diurnal dynamics of the gut microbiome. Cell Metab. *20*, 1006–1017.

Zmora, N., Zilberman-Schapira, G., Suez, J., Mor, U., Dori-Bachash, M., Bashiardes, S., Kotler, E., Zur, M., Regev-Lehavi, D., Brik, R.B., et al. (2018). Personalized Gut Mucosal Colonization Resistance to Empiric Probiotics Is Associated with Unique Host and Microbiome Features. Cell *174*, 1388–1405.

Please cite this article in press as: Tuganbaev et al., Diet Diurnally Regulates Small Intestinal Microbiome-Epithelial-Immune Homeostasis and Enteritis, Cell (2020), https://doi.org/10.1016/j.cell.2020.08.027

STAR★METHODS

KEY RESOURCES TABLE

REAGENT or RESOURCE	SOURCE	IDENTIFIER
Antibodies		
CD80	Biolegend	BioLegend Cat# 104738, RRID: AB_2564175
Ep-CAM	Biolegend	BioLegend Cat# 118218, RRID: AB_2098648
CD3e	Biolegend	BioLegend Cat# 100321, RRID: AB_389300
CD4	Biolegend	BioLegend Cat# 100540, RRID: AB_893326
CD8-a	Biolegend	BioLegend Cat# 100743, RRID: AB_2561352
CD8-b	Biolegend	BioLegend Cat# 126608, RRID: AB_961298
MHCII/I-E (MHCII)	Biolegend	BioLegend Cat# 107620, RRID: AB_493527
CD45	Biolegend	BioLegend Cat# 103147, RRID: AB_2564383
CD86	Biolegend	BioLegend Cat# 105007, RRID: AB_313150
TCR gamma delta	Biolegend	BioLegend Cat# 107508, RRID: AB_345266
CD4	Biolegend	BioLegend Cat# 100540, RRID: AB_893326
GATA3	Biolegend	BioLegend Cat# 653814, RRID: AB_2563221
T-bet	Biolegend	BioLegend Cat# 644804, RRID: AB_1595466
FoxP3	Biolegend	BioLegend Cat# 126406, RRID: AB_1089113
CD4	Biolegend	BioLegend Cat# 100421, RRID: AB_312706
CD3	Biolegend	BioLegend Cat# 300307, RRID: AB_314043
TCRb	Biolegend	BioLegend Cat# 109220, RRID: AB_893624
IL-5	Biolegend	BioLegend Cat# 504311, RRID: AB_2563161
IL-4	Biolegend	BioLegend Cat# 504104, RRID: AB_315318
IL-17A	Biolegend	BioLegend Cat# 506920, RRID: AB_961384
IL-10	Biolegend	BioLegend Cat# 505014, RRID: AB_493511
IFNg	Biolegend	BioLegend Cat# 505825, RRID: AB_1595591
MHCII/I-E (MHCII)	Biolegend	BioLegend Cat# 107608, RRID: AB_313323
Zombie-UV	Biolegend	Cat# 423108
TrueStain FCx (CD16/CD32)	Biolegend	BioLegend Cat# 101320, RRID: AB_1574975
Dapi	Sigma-Aldrich	Cat# D9542
E-Cadherin	BD Biosciences	BD Biosciences Cat# 612131, RRID: AB_2076677
Chemicals, Peptides, and Recombinant Proteins		
Vancomycin	Sigma-Aldrich	Cat# V1130
Ampicillin	Sigma-Aldrich	Cat# A1593
Metronidazole	Sigma-Aldrich	Cat# M3761
Neomycin	Sigma-Aldrich	Cat# N6386
Mouse rIL-10	Sigma-Aldrich	Cat# I3019

(*Continued on next page*)

Please cite this article in press as: Tuganbaev et al., Diet Diurnally Regulates Small Intestinal Microbiome-Epithelial-Immune Homeostasis and Enteritis, Cell (2020), https://doi.org/10.1016/j.cell.2020.08.027

Continued

REAGENT or RESOURCE	SOURCE	IDENTIFIER
Pitstop 2	Sigma-Aldrich	Cat# SML1169
CASIN	Sigma-Aldrich	Cat# SML 1253
Dynasore	Sigma-Aldrich	Cat# D7693
NAC	Sigma-Aldrich	Cat# A9165
Critical Commercial Assays		
HEK-Blue Detection	InvivoGen	Cat# hb-det3
HEK-Blue TLR2	InvivoGen	Cat# hkb-mtlr2
HEK-Blue TLR3	InvivoGen	Cat# hkb-mtlr3
HEK-Blue TLR4	InvivoGen	Cat# hkb-mtlr4
HEK-Blue TLR5	InvivoGen	Cat# hkb-mtlr5
HEK-Blue TLR7	InvivoGen	Cat# hkb-mtlr7
HEK-Blue TLR9	InvivoGen	Cat# hkb-mtlr9
HEK-Blue NOD1	InvivoGen	Cat# hkb-mnod1
HEK-Blue NOD2	InvivoGen	Cat# hkb-mnod2
HEK-Blue NULL2	InvivoGen	Cat# hkb-null2
HEK-Blue NULL1	InvivoGen	Cat# hkb-null1
HEK-Blue NULL1K	InvivoGen	Cat# hkb-null1k
HEK-Blue NULL1V	InvivoGen	Cat# hkb-null1v
HEK-Blue NULL2K	InvivoGen	Cat# hkb-null2k
Deposited Data		
Sequence data reported in this paper	European Nucleotide Archive	PRJEB38869
Experimental Models: Organisms/Strains		
SPF C57BL/6	The Jackson Laboratory	Stock No: 000664
SPF C57BL/6	WIS	SPF C57BL/6 WIS
SPF C57BL/6	Envigo	C57BL/6JOlaHsd
SPF SW	WIS	SPF SW WIS
GF C57BL/6	WIS	GF C57BL/6 WIS
GF SW	WIS	GF SW WIS
Villin-Cre (B6.Cg-Tg(Vil1 cre)1000Gum/J)	The Jackson Laboratory	Stock No: 021504
$Rag1^{-/-}$ (B6.129S7-Rag1tm1Mom/J)	The Jackson Laboratory	Stock No: 002216
$MHCII^{fl/fl}$	Steffen Jung & Pandelakis A. Koni (Hashimoto et al., 2002)	MHCII FL WIS
Per1/2DKO	Gad Asher (Bae et al., 2001)	PER1,2 DKO
Villin-Cre $MHCII^{fl/fl}$	WIS	MHCII KO WIS
Villin-Cre $MHCII^{fl/fl}$ $Rag1^{-/-}$	WIS	MHCII KO RAG1
OT-II (OTIIB6.CgTg(TcraTcrb)425Cbn/J)	The Jackson Laboratory	Stock No: 004194
CD4 KO ($Cd4^{tm1Mak}$)	The Jackson Laboratory	Stock No: 002663
SAA TKO	Kenya Honda (Atarashi et al., 2015)	SAA1,2,3 TKO
Villin-Cre $CDC42^{fl/fl}$	Nan Gao (Sakamori et al., 2014)	Villin-Cre $CDC42^{flox/flox}$
Oligonucleotides		
111-967F-PP: CNACGCGAAGAACCTTANC	Sigma-Aldrich	N/A
112-967F-UC3: ATACGCGARGAACCTTACC	Sigma-Aldrich	N/A
113-967F-AQ: CTAACCGANGAACCTYACC	Sigma-Aldrich	N/A
114-967F-S: CAACGCGMARAACCTTACC	Sigma-Aldrich	N/A

(*Continued on next page*)

Continued

REAGENT or RESOURCE	SOURCE	IDENTIFIER
115-1046R-S: CGACRRCCATGCANCACCT	Sigma-Aldrich	N/A
H2-AB1 probes library (Table S1)	Stellaris	N/A
EPCAM probes library (Table S2)	Stellaris	N/A
Software and Algorithms		
NIH's Database for Annotation, Visualization and Integrated Discovery	DAVID	https://david.ncifcrf.gov/
Gen Expression Omnibus	GEO	https://www.ncbi.nlm.nih.gov/geo/query/acc.cgi?acc=GSE23914
QIIMEII	QIIMEII	https://docs.qiime2.org/2020.6/
Trimmomatic	Usadellab	http://www.usadellab.org/cms/? page = trimmomatic
TopHat (v2.0.10)	JHU CCB	https://ccb.jhu.edu/software/tophat/index.shtml
HOMER	HOMER	http://homer.salk.edu
Meta Cycle	HughesLab	https://openwetware.org/wiki/HughesLab:JTK_Cycle
ImageJ	RSB NIH	https://imagej.nih.gov

RESOURCE AVAILABILITY

Lead Contact

Further information and requests for reagents may be directed to and will be fulfilled by Eran Elinav (eran.elinav@weizmann.ac.il).

Materials Availability

This study did not generate new unique reagents.

Data and Code Availability

The accession number for the sequence data reported in this paper is European Nucleotide Archive PRJEB38869.

EXPERIMENTAL MODEL AND SUBJECT DETAILS

Mice

C57BL/6 mice were purchased from Envigo and allowed to acclimatize to the animal facility environment for 2 weeks before used for experimentation. Germ-free C57BL/6 and Swiss Webster mice were born in the Weizmann Institute germ-free facility and routinely monitored for sterility. Villin-Cre (B6.Cg-Tg(Vil1-cre)1000Gum/J), OTII (OT-IIB6.CgTg(TcraTcrb)425Cbn/J), CD4 KO ($Cd4^{tm1Mak}$) and $Rag1^{-/-}$ (B6.129S7-Rag1tm1Mom/J) mice were obtained from the Jackson Laboratory. I-Ab fl/fl on a C57BL/6 background were kindly provided by Steffen Jung (Weizmann Institute) and Pandelakis A. Koni (Augusta University). Per1/2 DKO mice on a C57BL/6 background were kindly provided by Gad Asher (Weizmann Institute). SAA (1,2,3) triple knockout mice were kindly provided by Kenya Honda (Keio University). Villin-Cre CDC42 $^{fl/fl}$ mice were kindly provided by Nan Gao (Rutgers University). In all experiments, age- and gender-matched mice were used. Mice were 8-12 weeks of age at the beginning of experiments. All mice were kept at a strict 24-hour light-dark cycle, with lights being turned on from 6am to 6pm. For circadian experiments circadian cabinets (ActiMetrics) and software: ClockLab Analysis 6 (ActiMetrics); ClockLab Data Collection (ActiMetrics); ClockLab Chamber Control (ActiMetrics) were used to facilitate around the clock sample collection throughout two consecutive 24-hour cycles. In timed feeding experiments, food access was limited to the dark phase or light phase where indicated. Prior to any interventions, mice were randomized to ensure that no incidental pre-intervention differences in body weight existed between the different groups. Mice were exposed to high-fat diet for 4 weeks (Research Diets D12492) or normal chow diet (Envigo, Teklad 2018) as indicated. For antibiotic treatment, mice were given a combination of vancomycin (0.5 g/l), ampicillin (1 g/l), kanamycin (1 g/l), and metronidazole (1 g/l) in their drinking water for four weeks as previously described (Levy et al., 2015). All antibiotics were obtained from Sigma Aldrich. All experimental procedures were approved by the Weizmann Institute of Science IACUC.

Please cite this article in press as: Tuganbaev et al., Diet Diurnally Regulates Small Intestinal Microbiome-Epithelial-Immune Homeostasis and Enteritis, Cell (2020), https://doi.org/10.1016/j.cell.2020.08.027

METHOD DETAILS

Taxonomic Microbiome Analysis

Frozen SI luminal and mucosal microbiome samples were processed for DNA isolation using the DNeasy PowerLyzer PowerSoil kit (QIAGEN) according to the manufacturer's instructions. For the 16S rDNA gene PCR amplification, 1 ng of the purified fecal DNA was used for PCR amplification. Amplicons spanning the variable region V4 of the 16S rDNA gene were generated by using the following primers:Fwd 515F- AATGATACGGCGACCACCGAGATCTACACTATGGTAATTGTGTGCCAGCMGCCGCGGTAA, Rev 806R-CAAGCAGAAGACGGCATACGAGATXXXXXXXXXXXXAGTCAGTCAGCCGGACTACHVGGGTWTCTAAT, where X represents a barcode base. The reactions were subsequently pooled and cleaned (PCR clean kit, Invitrogen), and the PCR products were then sequenced on an Illumina MiSeq with 500 bp paired-end reads. Overlapping paired-end FASTQ files of 16S amplicon sequencing data were matched and analyzed using the Qiime2 pipeline (q2cli version 2019.7.0) (Bolyen et al., 2019). Data were demultiplexed according to sample-specific barcodes, poor quality bases were trimmed, sequences were denoised and binned to amplicon sequence variants (ASVs) using the dada2 plugin for Qiime2 (Callahan et al., 2016). Sequences were aligned using Mafft, masked and a phylogenetic tree was reconstructed with fasttree. Taxonomic assignment was performed using naive Bayes feature classifier and Greengenes 13_8 database. Community ecology analyses were carried out in R (v3.5.0). Data normalization was carried out by subsampling to the lowest sequencing depth in the respective experiment using the vegan package (v2.5-6, https://cran.r-project.org/web/packages/vegan/index.html) function rrarefy. Weighted UniFrac distances for ordination and clustering were calculated using the GUniFrac R package (v1.1, https://cran.r-project.org/web/packages/GUniFrac/index.html). Hierarchical clustering was performed using hclust function and Ward's minimum variance method. Differential abundance testing of individual bacterial genera was carried out with Mann-Whitney U test using the wilcox.test function, and log2 fold changes were calculated.

Library preparation for mcSCRB-seq

Library preparation of sorted SIEC was performed based on a previously published protocol (Bagnoli et al., 2018) with minor modifications. Specifically, 10,000 cells were collected and were resuspended in 20ul RLT buffer (QIAGEN, 79216) supplement with 40mM DTT. The cells solution was cleaned with 2X AM pure beads (Beckman Coulter) and reverse transcription was directly done on the cells with the beads using 20 u/μl Maxima H reverse transcriptase (Thermo, EP0753), 1mM dNTPS (Thermo R0182), 7.5% PEG 8000 (Sigma), 2 μM TSO E5V6NEXT (IDT) and 1 μL of 4nM barcoded RT primer for each reaction. The reaction was incubated at 42°C for 90 minutes inactivated at 80°C for 10 minutes. Finally, 1 μL of the reaction was diluted 1:20 with Tris-EDTA buffer (pH 8.0) and measured by real-time PCR using GAPDH primers as a house keeping gene to determine the Ct values of each sample. Samples with similar Ct values were pooled together, cleaned with 1X AM pure beads (Beckman Coulter) and eluted with 17 μL Tris-EDTA buffer (pH 8.0). The samples were then incubated with 1 μL of exonuclease I (20 u/μl) and 2 μL exonuclease buffer (Thermo, EN0582) and incubated 20 minutes at 37°C followed by 10 minutes at 80°C. cDNA amplification was performed by adding 1 μL of Terra polymerase (1.25u/μl) and 25 μL of Terra direct 2x buffer (Clontech, 639270), 1 μL of SINGV6 primer (10 μM, IDT) and 3 μL nuclease free water (Sigma, W4502). The PCR was done by 3 min 98°C, followed by 13-15 PCR cycles (for 0.5-3 ng/μl cDNA after amplification) of 15 s 98°C, 30 s 65°C, 68°C 4 min. Final elongation was performed for 5 minutes, 72°C. The cDNA products were cleaned using 0.8X AM pure beads (Beckman Coulter) and eluted with 10 μL Tris-EDTA buffer (pH 8.0). cDNA (0.8-2 ng/μl) was further used to construct Nextera XT DNA libraries (Illumina, FC-131-1024) following manufacturer's instructions and 3′ ends were enriched with a custom P5 primer (P5NEXTPT5, IDT) and amplified with i7 index primers from Nextera XT Index Kit v2 (Illumina, FC-131-1002). Finally, the amplified libraries were cleaned using 0.6X AM pure beads (Beckman Coulter) and eluted with 20 μL of Tris-EDTA buffer (pH 8.0). The quality control of the resulting libraries was performed with an Agilent High Sensitivity D1000 ScreenTape System (Agilent, 5067- 5584). Libraries that passed quality control were loaded with a concentration of 2 pM on 75 cycle high output flow cells (Illumina, FC-404-2005) and sequenced on a NextSeq 500 (Illumina) with the following cycle distribution: 8bp index 1, no index 2, 16bp read 1, 66bp read 2.

mcSCRB-seq analysis

Raw files were converted to fastq files using the bcl2fatq package (Illumina). i7 barcodes were then used for pool demultiplexing. zUMIs package (https://doi.org/10.1101/153940) was used for samples demultiplexing, STAR alignment to the mouse genome (GRCm38.84), and unique UMI counting. For each comparison, genes with #reads $\geq$ 10e-4 of total reads, expressed in at least 1/5 of one group in each comparison were included for the analysis.

DE genes were found using DESeq2 models fitted separately for each comparison (Figure 1A; Figures S1B–S1D, Figure S2A). Normalized gene expression values (Figures S1B–S1D; Figure S2A) were calculated using the regularized log transformation (rlog). Gene assignment to GO terms was done in the following manner: For each gene, -log(padj) sign(log2FoldChange) scores were calculated. Then the bulk.gsea function (liger package http://ge-lab.org/gskb/2-MousePath/MousePath_GO_gmt.gmt) was used as the universe model.

Single-molecule fluorescence *in situ* hybridization (smFISH)

Collected murine tissues were flushed with PBS, fixed in 4% paraformaldehyde (PFA) in PBS for 3 hours and subsequently agitated in 30% sucrose, 4% PFA in PBS overnight at 4°C. Fixed tissues were embedded in OCT (Tissue-Tek), 8 μm sections were used for smFISH staining. Probe libraries (Tables S2 and S3) were designed using the Stellaris FISH Probe Designer (Biosearch Technologies,

Inc., Petaluma, CA). The intestinal sections were hybridized with smFISH probe sets according to a previously published protocol. Dapi (Sigma-Aldrich, D9542) and a FITC-conjugated antibody against E-Cadherin (BD Biosciences, 612131) were utilized as nuclear and cell-membrane counterstains, respectively. SmFISH imaging was performed on a Nikon-Ti-E inverted fluorescence microscope with a 100 × oil-immersion objective and a Photometrics Pixis 1024 CCD camera using MetaMorph software as previously reported . The epithelial cell fragments were manually segmented based on nuclear and cell-membrane counterstains and mRNA density (number of mRNA per unit cell segment volume) was computed using custom MATLAB program (*28*, MATLAB Release 2016a, The MathWorks Inc., USA). We used FIJI software to extract the intensity profiles along manually marked lines spanning the basal to apical cell axis. A previously reported FIJI script was used to extract the intensity profiles along these lines for each channel and for each stack using the getProfile command. Using MATLAB, we identified the basal and apical parts of the line segments according to the line intensity profile of the DAPI channel, where the proximal and distal line segments that were below 0.7 of the maximum were defined as basal and apical sides respectively. We next removed background intensity, defined as the lower percentile of the line profiles and computed the ratio between the maximal intensities in the apical and basal sides.

Image analysis

Images of tissue sections were taken with a confocal microscope Fluorview FV1200 using Kalman and sequential laser emission to reduce noise and signal overlap. Scale bars were added to each image using the confocal software FV10-ASW 3.1 Viewer. Images were analyzed and visualized using ImageJ software (Schneider et al., 2012).

Flow Cytometry Analysis (FACS)

SI samples were extensively washed from the luminal content and opened longitudinally. The tissue was then cut into pieces of 1cm length and incubated in HBSS containing 2mM EDTA and 1mM DTT at 37°C for 15 minutes while shaking at 180 rpm. Epithelial cells were collected, filtered, centrifuged, and subsequently stained with the Zombie-UV viability dye at room temperature protected from light for 15 minutes, followed by a wash with PBS containing 1% BSA (FACS buffer), FC-receptors blocking and surface markers staining on ice for 30 minutes. Following the separation from epithelium, the lamina propria samples were digested using DNAase I and Collagenase II (Sigma). The isolated cells were washed with cold PBS and resuspended in FACS buffer for direct cell surface staining. Intracellular staining with antibodies against transcription factor targets was performed on cells fixed using Foxp3 Intracellular Staining Kit (eBioscience) according to the manufacturer's instructions, while intracellular staining with antibodies against cytokines was performed on *in vitro* re-stimulated cells using Cell Activation Cocktail with Brefeldin A (Biolegend) and fixed with 4% PFA in PBS for 15 minutes at room temperature protected from light. Multiparameter analysis was performed on a LSR II or LSR Fortessa (BD) and analyzed with FlowJo software (Tree Star).

Ussing chamber

Transepithelial resistance was measured a modular Ussing chamber system (Warner Instruments, P2300) according to the manufacturer's instructions as in Thaiss et al. (2018). In brief, EasyMount chambers were calibrated, SI tissue was excised from mice and immediately mounted, and voltage clamp measurements were performed. Tissues were maintained at 37°C in physiological salt solution throughout the duration of the recordings.

Measuring Colonic Epithelial Barrier Permeability by FITC-dextran

On the day of the assay, 4 kDa fluorescein isothiocyanate (FITC)-dextran was dissolved in phosphate buffered saline (PBS) to a concentration of 40 mg/ml. Mice were fasted for 4 hours prior to gavage with 200 μL of dextran. Mice were anesthetized and 3 hours following gavage peripheral blood was collected, excitation wavelength of 485 nm and emission wavelength of 535 nm.

Quantification of microbial products at systemic sites

The following PRR reporter cell lines were obtained from InvivoGen (HEK-Blue TLR and NLR Reporter cell lines): TLR2, TLR3, TLR4, TLR5, TLR7, TLR9, NOD1, NOD2. Extracts from liver, portal vein serum and peripheral blood serum were homogenized and added to reporter cell lines incubated with HEK-Blue detection medium (InvivoGen) according to the manufacturer's instructions as in Thaiss et al. (2018).

Purification of intestinal epithelial cells for RNA isolation

Intestinal tissue was excised from mice, thoroughly rinsed with ice-cold PBS to clean the tissue from luminal content and opened longitudinally. The tissue was then cut into pieces of 1cm length and incubated in HBSS containing 2mM EDTA and 1mM DTT at 37°C for 15 minutes while shaking at 180 rpm. Epithelial cells were collected, filtered, centrifuged, and subsequently stained with the Zombie-UV viability dye at room temperature protected from light for 15 minutes, followed by a wash with FACS buffer, FcR blocking and anti-EpCAM, anti-CD45 staining on ice for 30 minutes. Cells were then washed, resuspended, filtered and sorted into lysis/binding buffer (Life Technologies) using a FACS-Fusion cell sorter (BD).

Treatment with chemical inhibitors in externalized intestinal loops

Perfusion of extra-intestinal loops was done as previously described (Ladinsky et al., 2019). Briefly, mice were anesthetized using ketamine (40 mg/kg) and xylazine (5 mg/kg). A 6 cm portion of the distal jejunum was exteriorized and the contents flushed. The exter-

Please cite this article in press as: Tuganbaev et al., Diet Diurnally Regulates Small Intestinal Microbiome-Epithelial-Immune Homeostasis and Enteritis, Cell (2020), https://doi.org/10.1016/j.cell.2020.08.027

nalized portion was perfused with the inhibitors for 30 min using a syringe pump. Animals were perfused with 20 mM Pitstop 2 (SIGMA SML1169), 10 mM CASIN (SIGMA SML 1253), 50 uM Dynasore (SIGMA D7693), or buffer. Mice were anesthetized throughout the experiment and kept warm by heating pads linked to thermoregulators (Harvard Apparatus Homeothermic Monitoring System Model 55-7020) that sense and maintain body temperature. After perfusion, the perfused section, were collected and processed for FACS.

Bacterial isolation

Fresh anaerobic mucosal distal jejunum samples from metronidazole- and vancomycin- treated mice (Figure 1C) were cultured anaerobically and aerobically using 31 media (Table S4) for culture-enriched molecular profiling as described previously (Lau et al., 2016). The cultivable portion of the mucosal microbiota was determined by comparing the operational taxonomic units (OTUs) recovered by 16S sequencing of the culture plates to OTUs from culture-independent sequencing of the microbiome sample.

Fecal Microbiome Transplantation (FMT)

All FMT procedures were carried out as fast as possible to avoid prolonged exposure to oxygen. All collections were carried out within a laminar flow hood. Microbiome sample collection: Microbiome samples were collected in 2ml tubes (Eppendorf) containing sterile 20% glycerol. Following sample transfer into glycerol solution, the microbiome matter was homogenized. After homogenization the samples were immediately placed on dry ice prior to long-term storage at –80°C. Microbiome transfer: Following thawing, 0.1g of fecal sample was mixed in 1 mL sterile PBS, filtered and immediately placed in a Gaspak EZ Anaerobe System (BD) prior to oral gavage with 200 μL of a diluted microbiome sample per mouse.

Adoptive T cell transfer mediated enteritis

Spleen T effector cells ($CD4^+CD25^-CD45RB^{HI}$) were sorted and 0.3ml of the cell suspension was injected i.p. at the concentration $5*10^6$ cells/ml into Villin-Cre $MHCII^{fl/fl}$ $Rag1^{-/-}$ versus $MHCII^{fl/fl}$ $Rag1^{-/-}$ littermate mice, as described previously (Powrie et al., 1994), to trigger pan enteritis (Eri et al., 2012). Weight measurements were conducted twice weekly. Three weeks post T cell transfer intestinal permeability was assessed using FITC-dextran. In the IL-10 rescue experiment mice were intraperitoneally injected with 4 μg of recombinant IL-10 (Sigma) in 100 μL of PBS or with vehicle alone (Flannigan et al., 2014; Kunisawa et al., 2013). Injections were performed every three days starting from day 21 on days 21, 24, 27, 30, 33 and 36 post adoptive transfer. Mice were euthanized four weeks post T cell transfer and histological, Ussing chamber measurements and FACS analysis of the ileum and distal jejunum were performed.

Treatment with rIL–10

Intraperitoneal injections of 4 μg of recombinant IL-10 (Sigma) in 100 μL of PBS or with vehicle alone (Flannigan et al., 2014; Kunisawa et al., 2013) were carried out twice weekly for two weeks prior to mice euthanization, Ussing chamber measurements and FACS analysis of the ileum and distal jejunum. Measurements of FITC-dextran concentration in peripheral blood samples were done 3 days prior to mice euthanization.

Histology

Ileum sections were fixed in paraformaldehyde and embedded in paraffin for staining with H&E. Subsequently, sections were examined by a blinded veterinary pathologist and scored for transmural inflammation, dense infiltrates involving neutrophils, and crypt abscessation on a scale from 0 (healthy) to 4 (most severe).

Data integrity check

Figure and supplementary figure panels were checked for data integrity using the Proofig pipeline.

QUANTIFICATION AND STATISTICAL ANALYSIS

Data are expressed as mean ± SD. Comparisons made between two groups were performed using Mann-Whitney U-test. ANOVA with Tukey's post hoc test were used for comparisons between multiple groups. Cycling behavior was assessed using the Meta_cycle package (Wu et al., 2016), with oscillations tested for a 24-hour period length. For experiments shorter than 30 hours, we evaluated the significance of the periodic trend using 100 cross validations (CV), in which the data was split to train (70%) and test (30%) groups, a periodic model $A\sin(T+C)$ was trained on the training dataset (where T represents the time variable, and parameters A and C are learned by minimizing the L2 norm of the objective from the ground truth). For the test dataset, we set T_{obs} as the mean square error (MSE) from the fitted model, then for 1000 permutations we set T_i to hold the MSE of the shuffled testing group from the fitted model. For each CV round, we set $p_j \leftarrow \#\{i \text{ such that } T_i \leq T_{obs}\}/1001$ and report the mean p_j across all CV rounds. To test for rhythmicity in experiments longer than 30 hours, for pulled experiments we used the Lomb-Scargle (LS) method (Glynn et al., 2006; Lomb, 1976), and for individual repetitions we used JTK_CYCLE (Hughes et al., 2010), both implemented in MetaCycle package. The data was averaged per time point. Linear regression was used to assess correlations between two datasets. Unless stated otherwise, elements with $p < 0.05$ and $q < 0.1$ were considered significant. *$p < 0.05$, **$p < 0.01$, ***$p < 0.001$, ****$p < 0.0001$

Supplemental Figures

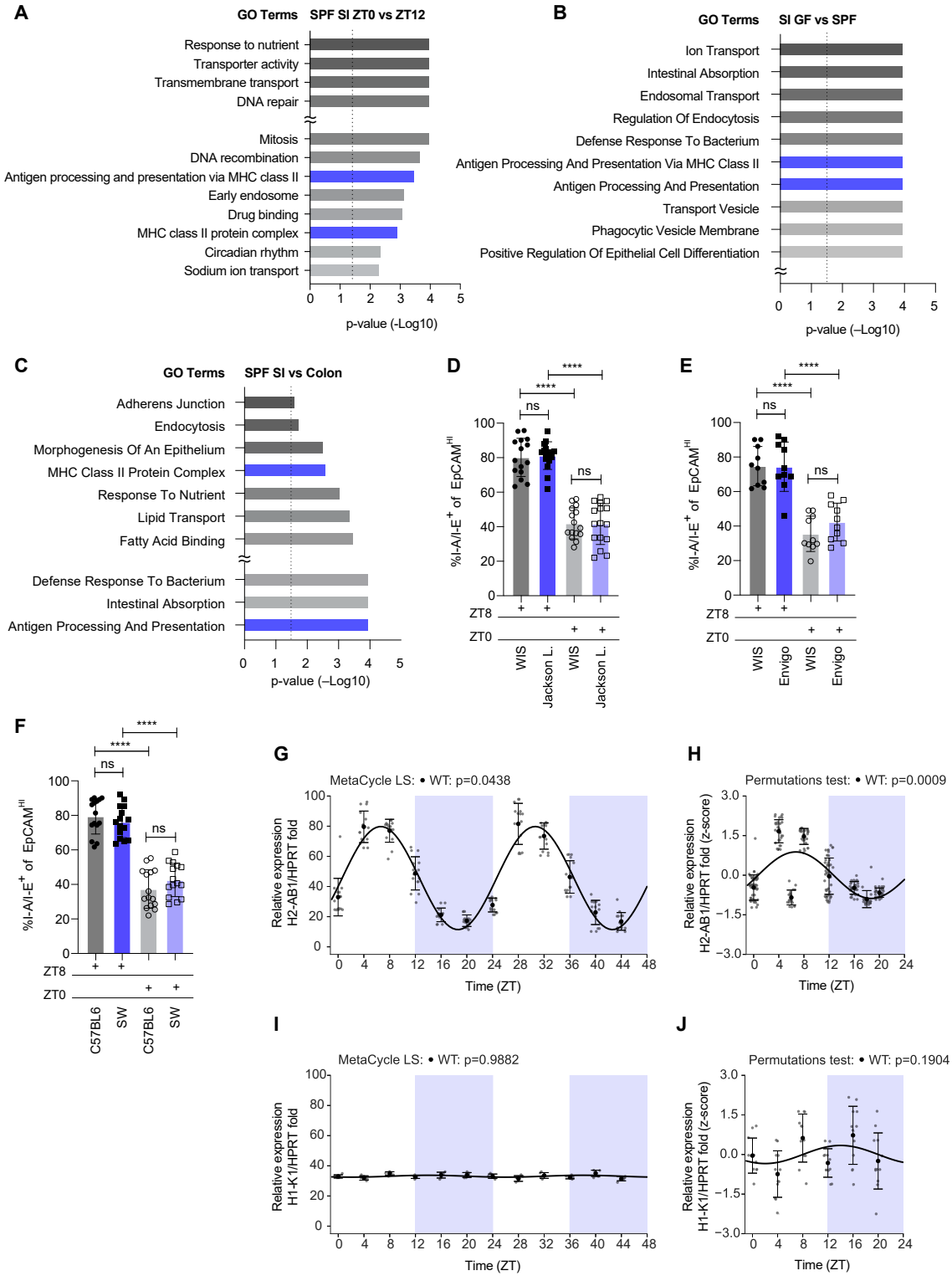

(legend on next page)

Figure S1. SIECs MHCII Expression Adapts to Dietary and Microbiome Cues in a Time of Day-Specific Manner, Related to Figure 1

(A-C) Significantly different expression of GO terms in sorted epithelial cells in the following conditions: ZT0 versus ZT 12 (A), GF versus SPF (B) and SPF SI versus colon (C). Significance: $q < 0.1$. Wilcoxon rank sum with FDR correction. (D-F) Frequency of $MHCII^{+}CD45^{-}EpCAM^{hi}$ SIECs (D) from distal jejunum of C57BL6 mice housed in WIS, Israel versus Jackson Laboratory, USA vivaria at ZT0 versus ZT8; (E) from distal jejunum of C57BL6 mice housed in WIS, Israel versus Envigo, Israel vivaria versus Envigo, Israel at ZT0 and ZT8; (F) from distal jejunum of C57BL6 versus Swiss Webster outbred mice housed in WIS vivarium, Israel at ZT0 versus ZT8. All data represents at least two independent experiments. (G-F) mRNA expression of $MHCII^{+}$ (*H2-Ab1*, G-H), *H1-K1* (I-J) in isolated $CD45^{-}EpCAM^{hi}$ SIECs from distal jejunum examined every 4 hours across 48h (G,I) and in an average of two consecutive 24h (H,J). The line represents the sine fit curve and p values were calculated by LS test for 48h (G,I) or by PT for 24h (H,J). Means ± SD are plotted. $^{*}p < 0.05$, $^{**}p < 0.01$, $^{***}p < 0.001$, $^{****}p < 0.0001$ by Mann-Whitney U test.

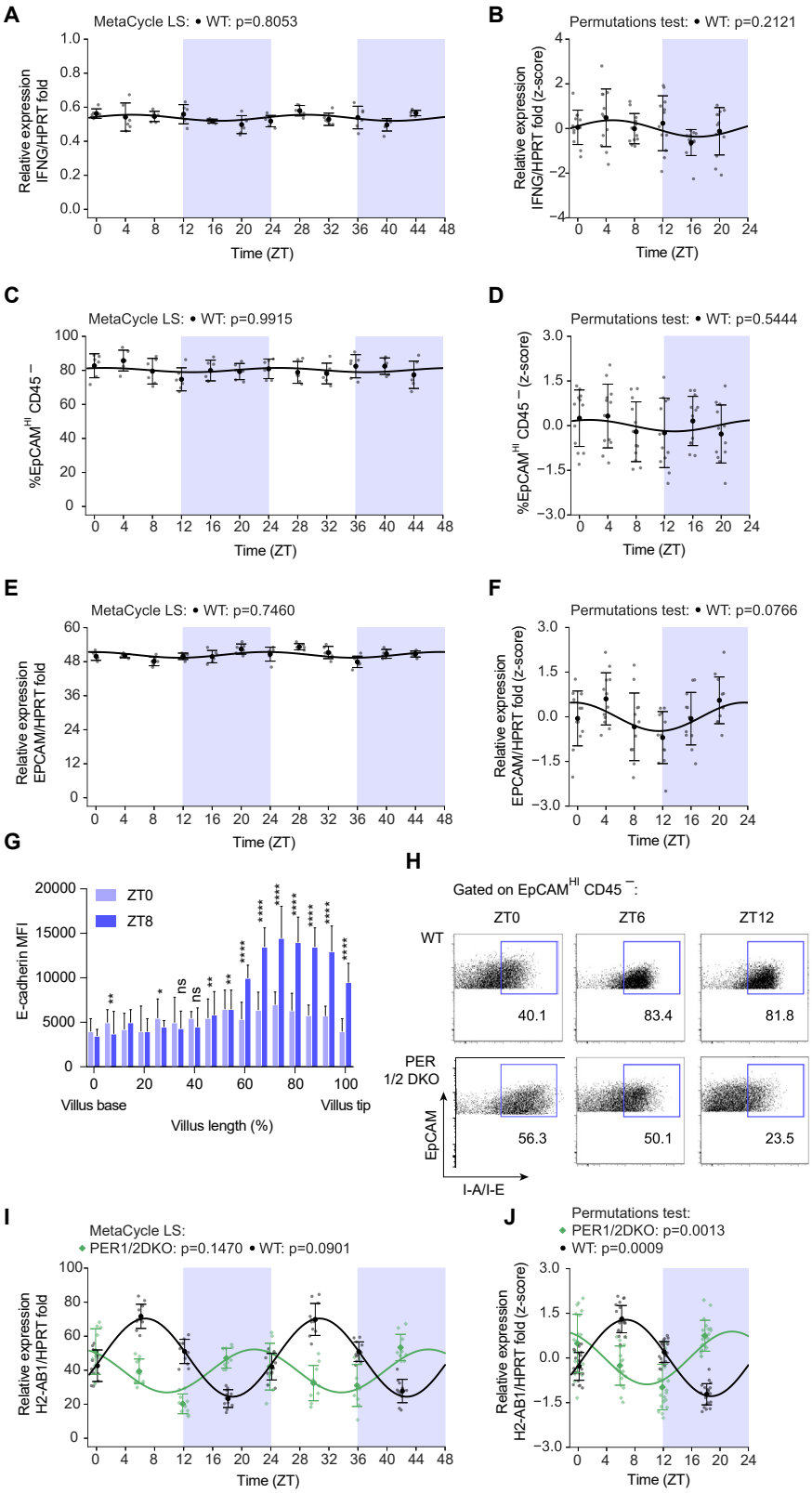

(legend on next page)

Figure S2. SIECs MHCII, but Not MHCI, Exhibit a Diurnal Pattern of Expression, Related to Figures 1 and 2

(A-B) mRNA expression of *Ifng*, (C-D) frequency of EpCAM^{hi}CD45^{-} cells and (E-F) mRNA expression of *EPCAM* in isolated CD45^{-}EpCAM^{hi} SIECs from distal jejunum examined every 4 hours across 48 h (A,C,E) and in an average of two consecutive 24 h (B,D,F). The line represents the sine fit curve and p values were calculated by LS test for 48 h (A,C,E) or by PT for 24 h (B,D,F). (G) MFI of E-Cadherin alongside the length of villi in distal jejunum at ZT0 versus ZT8. $p < 0.05$, $^{**}p < 0.01$, $^{***}p < 0.001$, $^{****}p < 0.0001$ by 2-way ANOVA. (H) FACS plots of SIEC isolated from Per1/2DKO and WT mice across 48 h. (I-J) mRNA expression of *H2-AB1* of SIECs isolated from distal jejunum of Per1/2 DKO versus WT mice examined every 4 hours across 48 h (I) and in an average of two consecutive 24h (J). The line represents the sine fit curve, p values were calculated by LS test for 48 h (I) or by PT for 24 h (J).

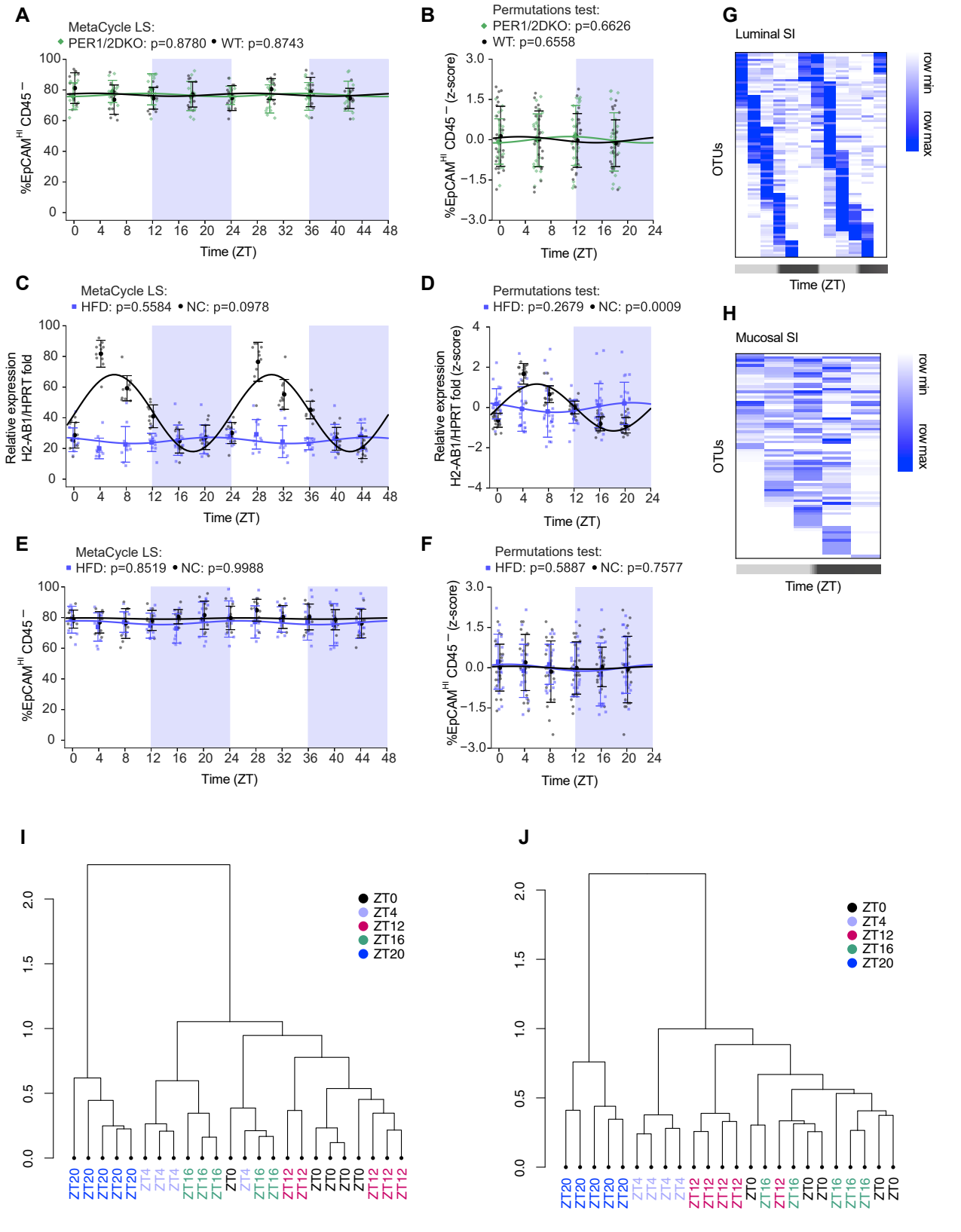

(legend on next page)

Figure S3. The Luminal and Mucosal SI Microbiome Undergoes Time of Day-Specific Compositional Changes, Related to Figures 2 and 3

(A-B) frequency of EpCAM^{hi}CD45^{-} cells of SIECs isolated from distal jejunum of Per1/2 DKO versus WT mice examined every 4 hours across 48 h (A) and in an average of two consecutive 24 h (B). The line represents the sine fit curve, p values were calculated by LS test for 48 h (A) or by PT for 24 h (B). (C-D) mRNA expression of *H2-AB1*, and (E-F) frequency of EpCAM^{hi}CD45^{-} cells of SIECs isolated from distal jejunum of HFD versus NC fed mice examined every 4 hours across 48 h (C,E) and in an average of two consecutive 24 h (D,F). The line represents the sine fit curve, p values were calculated by LS test for 48 h (C,E) or by PT for 24 h (D,F). (G-H) Heatmap representation of the most significantly oscillating bacterial OTUs, MetaCycle, luminal SI microbiome (G), mucosal SI microbiome (H). (I–J) Temporal clustering of luminal SI microbiome (I), mucosal SI microbiome (J).

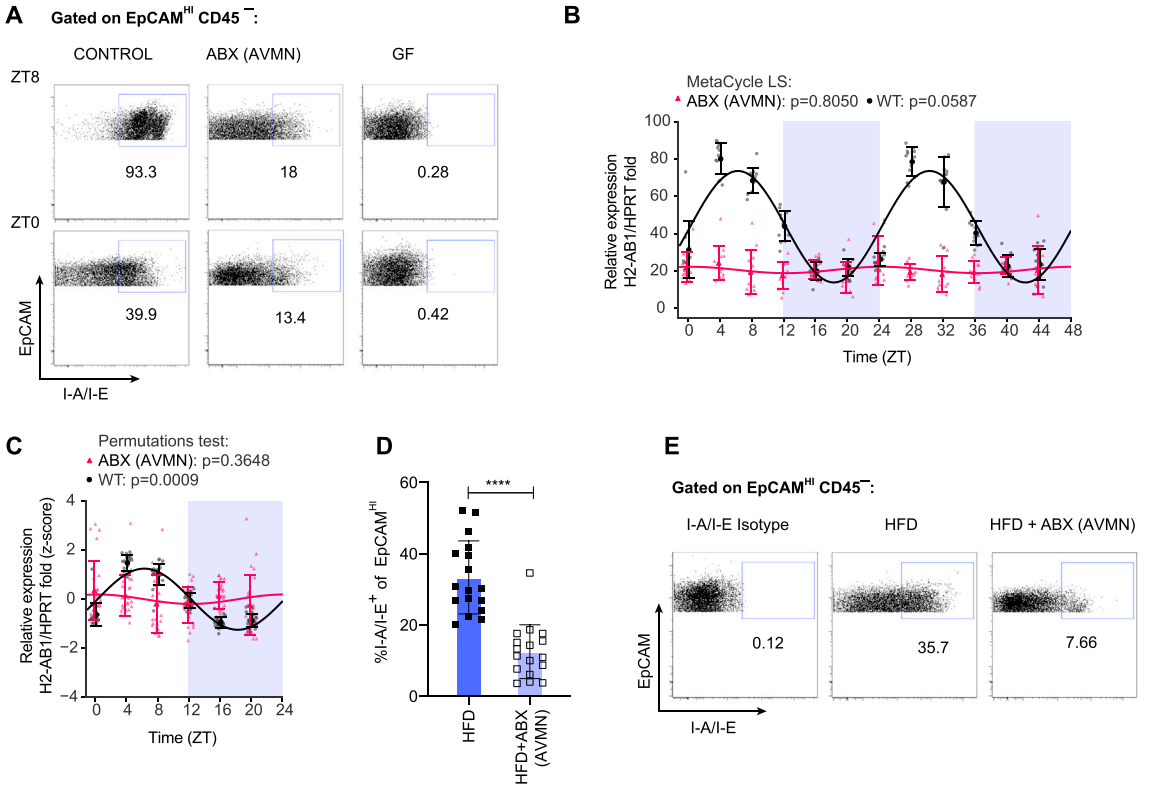

(legend on next page)

Figure S4. Diurnal Pattern of SIECs MHCII Expression Is Sustained through Interactions with Distinct Mucosal Bacteria, Related to Figures 3 and 4

(A) FACS plots of SIEC isolated from antibiotics-treated mice (ABX, AVMN cocktail) and germ- free (GF) and control SPF mice at ZT0 versus ZT8. (B-C) mRNA expression of *H2-AB1* of SIECs isolated from distal jejunum of ABX-treated versus control mice across 48 h (B) and in an average of two consecutive 24 h (C). (D-E) Frequency of CD45–EpCAM^{hi} SIECs from distal jejunum of HFD mice treated with ABX (AVMN cocktail). All data represents at least two independent experiments. Means ± SD are plotted. *$p < 0.05$, **$p < 0.01$, ***$p < 0.001$, ****$p < 0.0001$ by Mann-Whitney U test. (F–J) Volcano plots of SI luminal microbiome composition upon various antibiotics treatment (F–I), and HFD (J) collected at ZT0.

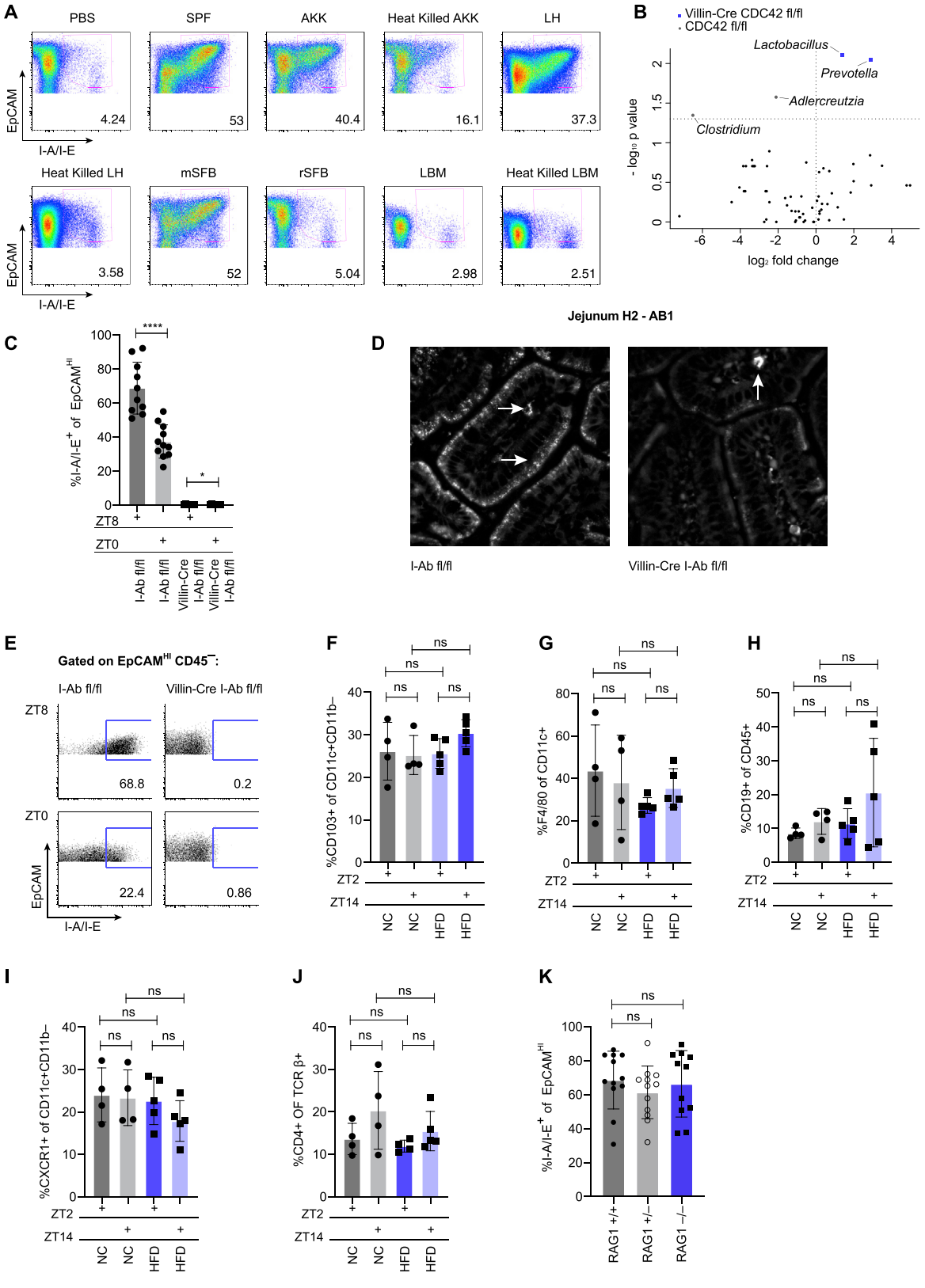

(legend on next page)

Figure S5. Populations of "Professional" SI Antigen Presenting Cells Remain Unaffected by High Fat Diet, Related to Figures 4 and 5

(A) Representative FACS plots of MHCII+CD45–EpCAM^{hi} SIECs of germ-free (GF) mice mono-colonized with different microbiome content based on the culturomics results composition (16S-rDNA Sequencing). (B) A volcano plot of luminal microbiome composition of Villin-cre CDC42 fl/fl versus CDC42 fl/fl littermate controls. (C-E) Frequency of MHCII+CD45–EpCAM^{hi} cells (C), MHCII expression in SI villi with arrows highlighting expression by SIECs at the periphery of the villi and "professional" APC at the center of villi (D) and representative FACS plots (E) of SIECs isolated from the distal jejunum of Villin-cre I-Ab fl/fl versus I-Ab fl/fl control mice at ZT0 versus ZT8. (F-J) Frequency of CD103+ of CD11c+CD11b– (F), F4/80+ of CD11c+ (G), CD19+ of CD45+ (H) CXCR1+ CD11c+CD11b– (I), and CD4+ TCRβ (J) were tested in the lamina propria of NC- and HFD-fed WT mice at ZT2 and ZT14. (K) Frequency of MHCII+CD45–EpCAM^{hi} SIECs from the distal jejunum of RAG1–/– mice versus Rag1+/– and WT littermate controls. All data represents at least two independent experiments. Means ± SD are plotted. *$p < 0.05$, **$p < 0.01$, ***$p < 0.001$, ****$p < 0.0001$ by Mann-Whitney U test.

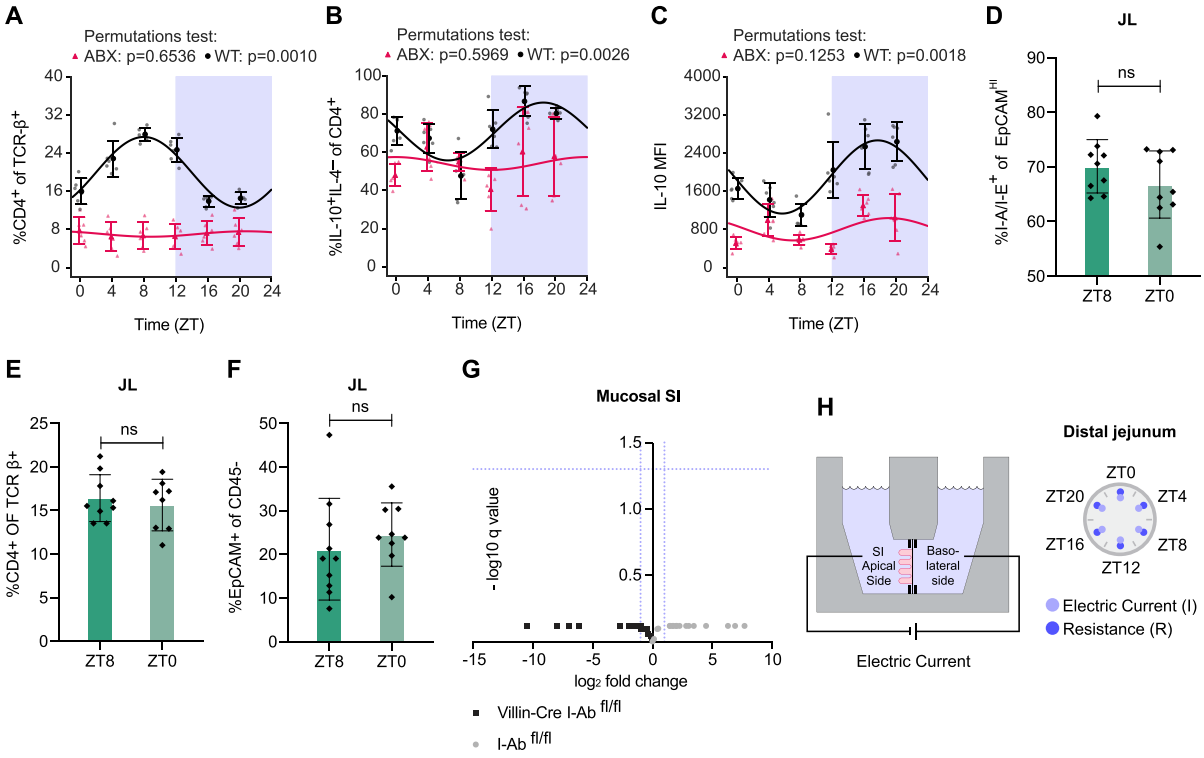

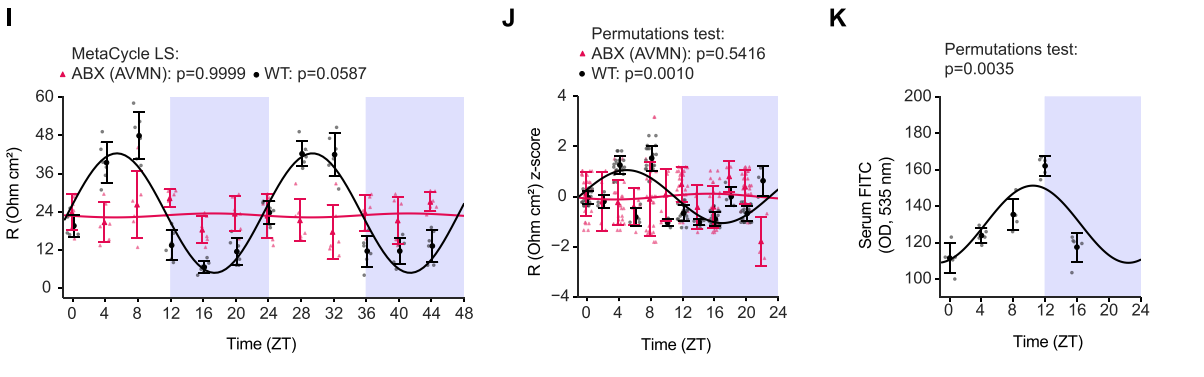

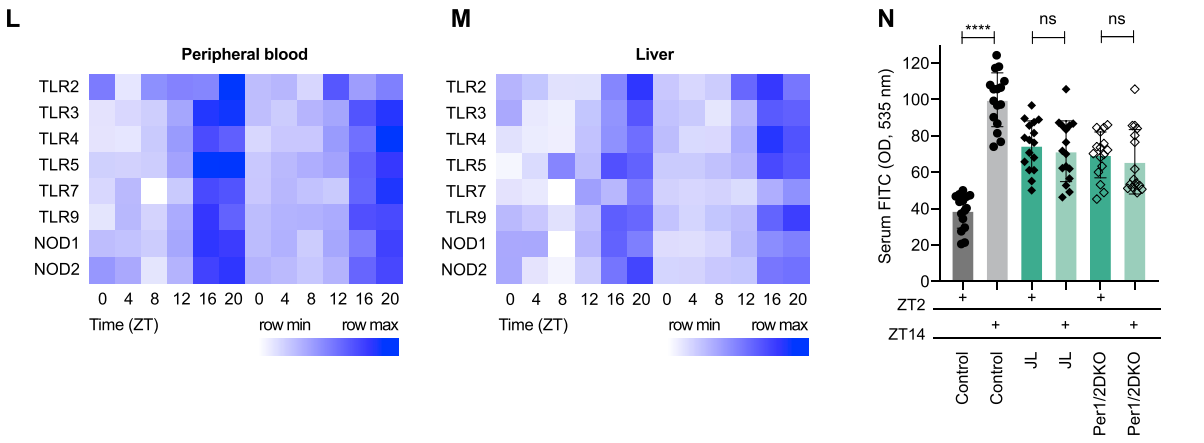

(legend on next page)

Figure S6. Small Intestinal Permeability Oscillates in a Time of Day-Specific Manner, Related to Figures 5 and 6

(A-C) Frequency of CD4+ IEL (A), frequency IL-10+ IELs (B) and IL-10 MFI of CD4+ IEL (C) every 4 hours throughout a 24-hour cycle. The line represents the sine fit curve, p values were calculated by permutation test (A–C). (D-F) Frequency of MHCII (D), CD4+ IEL (E) and EpCAM^{hi} cells (F) in jet-lag (JL) mice compared to WT controls at ZT0 versus ZT8. (G) Mucosal SI microbiome composition of Villin-Cre I-Abfl/fl mice versus I-Abfl/fl littermate control mice. (H) Schematic presentation of SI ion permeability and trans-epithelial resistance measurement by the Ussing chamber every 4 hours throughout two consecutive 24 h cycles. (I-J) Trans-epithelial resistance of ABX-treated mice (AVMN cocktail) versus WT control mice examined for 48 h (I) and in an average of two consecutive 24 h (J). (K) SI permeability measured by concentration of FITC-coated 4kDa dextran beads examined every 4 hours for a period of 24 hours. (L-M) PRR ligand concentrations utilizing a reporter cell assay examined in the peripheral blood serum (L) and the liver (M). Samples were collected every four hours for two consecutive 24-hour cycles. (N) Concentration of FITC- dextran beads of jet-lag and PER1/2 DKO mice versus their littermate WT controls at ZT2 versus ZT14. All data represents at least two independent experiments. Means ± SD are plotted. *$p < 0.05$, **$p < 0.01$, ***$p < 0.001$, ****$p < 0.0001$ by Mann-Whitney U test.

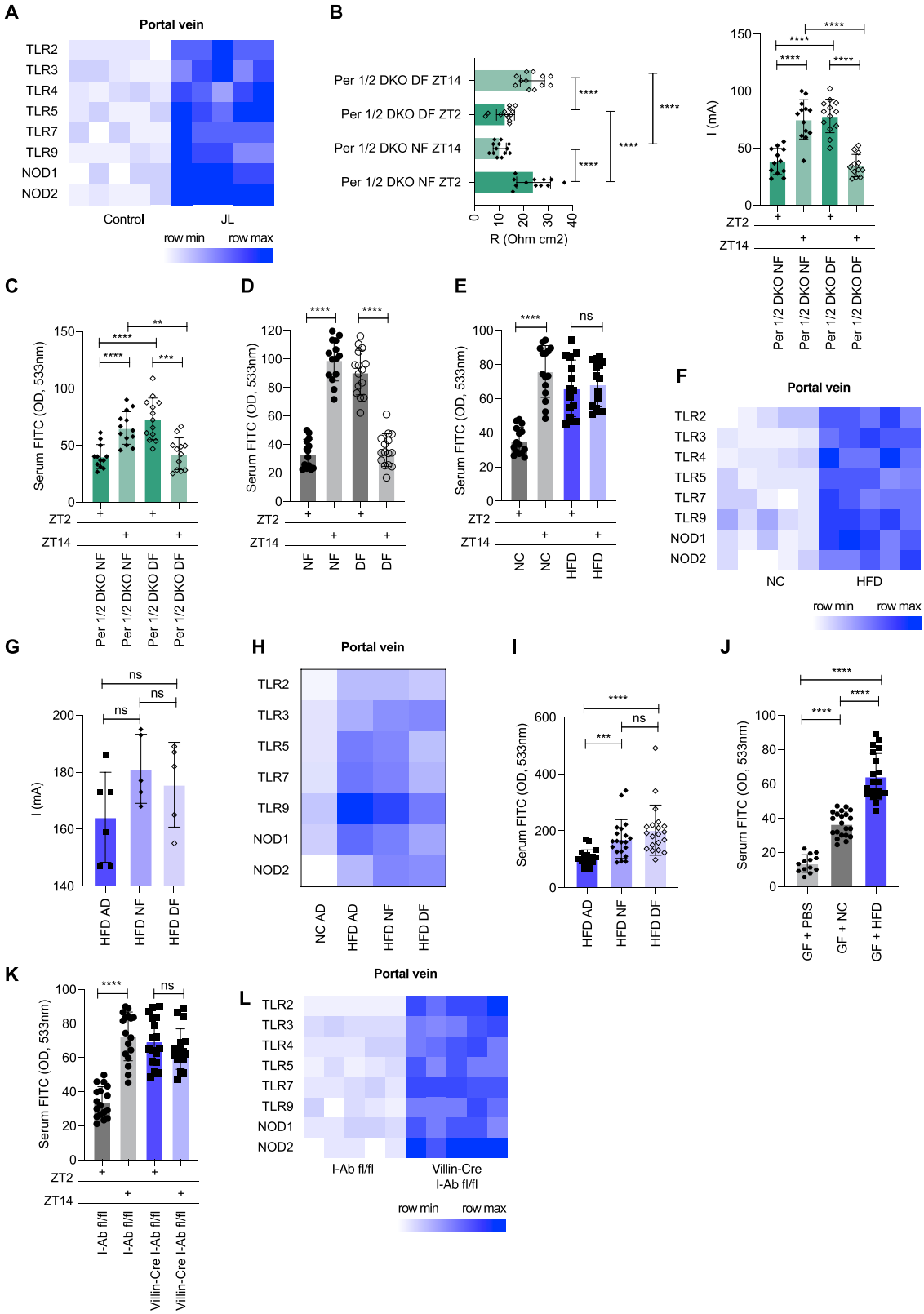

(legend on next page)

Figure S7. Temporal Pattern of SI Permeability Is Regulated by the Timing of Food Intake and Food Content, Related to Figure 6

(A) PRR ligand concentrations of jet lag mice versus control mice in the portal vein. (B-C) Ion permeability and trans-epithelial resistance (B) and concentration of FITC- dextran beads (C), of PER1/2 DKO mice day fed (DF) or night fed (NF) at ZT2 versus ZT14. (D) Concentration of FITC-coated 4kDa dextran beads of WT mice fed during the day (DF) or night (NF) at ZT2 versus ZT14. (E) Concentration of FITC- dextran beads of HFD versus NC mice examined at ZT2 versus ZT14. (F) PRR ligand concentrations of NC versus HFD mice in the portal vein. (G-I) SI ion permeability (G), PRR ligand concentrations (H) and MFI of FITC- dextran beads (I) of HFD mice fed ad libitum (AD), night-fed (NF) or day-fed (DF). (J) Concentration of FITC- dextran beads of germ-free mice colonized with fecal content of HFD, NC mice or gavaged with PBS. (K) Concentration of FITC- dextran beads of Villin-Cre I-Abfl/fl mice versus I-Abfl/fl littermate control mice at ZT2 versus ZT14. (L) Portal vein PRR ligand concentrations of Villin-Cre I-Abfl/fl mice versus I-Abfl/fl littermate controls. All data represents at least two independent experiments. Means ± SD are plotted. *$p < 0.05$, **$p < 0.01$, ***$p < 0.001$, ****$p < 0.0001$ by Mann-Whitney U test.

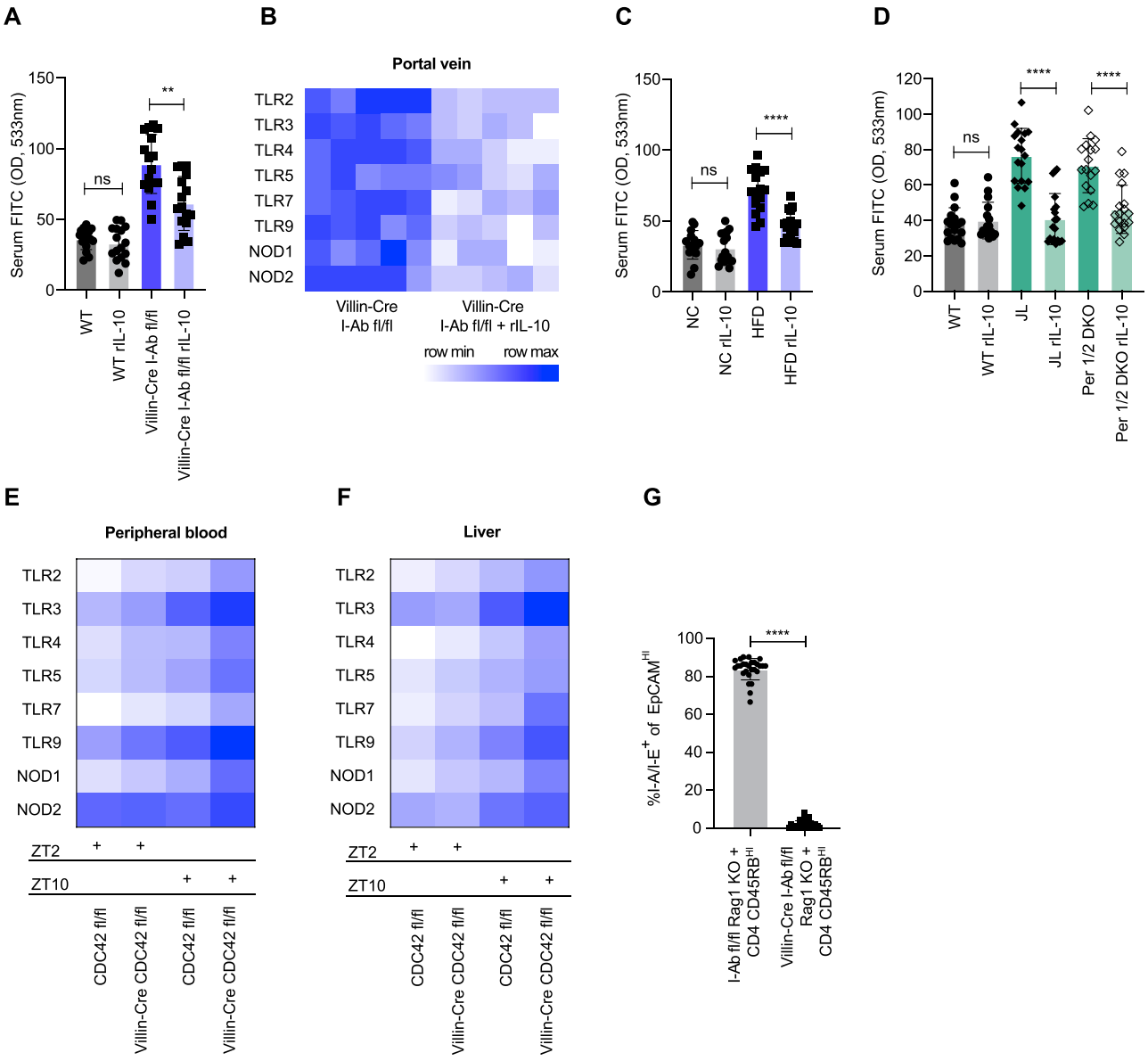

Figure S8. IL-10 Regulates SI Permeability Related to Figures 6 and 7

(A-B) Concentration of FITC- dextran beads (A) and portal vein PRR ligand concentrations (B) of Villin-Cre I-Abfl/fl mice versus I-Abfl/fl littermate controls supplemented with recombinant IL-10 (rIL-10). (C), (D) Concentration of FITC- dextran beads of HFD versus NC mice (C), jet-lag and PER1/2 DKO mice (D) supplemented with recombinant IL-10. (E), (F) PRR ligand concentrations from peripheral blood serum (E) or liver (F) of Villin-cre CDC42fl/fl mice versus CDC42fl/fl littermate control mice. (G) Frequency of MHCII+CD45–EpCAM^{hi} SIECs in Villin-cre I-Ab fl/fl Rag1–/– versus I-Ab fl/fl Rag1–/– littermate mice systemically administered with CD4+CD45RB^{hi} lymphocytes. All data represents at least two independent experiments. Means ± SD are plotted. *$p < 0.05$, **$p < 0.01$, ***$p < 0.001$, ****$p < 0.0001$ by Mann-Whitney U test.